NGU Report 2010.049
Gravity and magnetic data acquisition over a segment of the Møre-Trøndelag Fault Complex

Geological Survey of Norway
NO-7491 Trondheim, Norway
Tel.: 47 73 90 40 00
Telefax 47 73 92 16 20

REPORT

Report no.: 2010.049 | ISSN 0800-3416 | Grading: Open

Title: Gravity and magnetic data acquisition over a segment of the Møre-Trøndelag Fault Complex

Authors:
Aziz Nasuti, Majid Beiki, Jörg Ebbing

Client:

County:
Sunndalsøra

Commune:
Møre and Romsdal

Map-sheet name (M=1:250.000)

Map-sheet no. and -name (M=1:50.000)
1320 and 1420

Deposit name and grid-reference:

Number of pages: 48 Price (NOK): 200,-
Map enclosures:

Fieldwork carried out:
August 2008

Date of report:
10/09/2010

Project no.:
3184.00

Person responsible:

Summary:

Gravity and magnetic data were acquired in the area of Eidsøra, close to Tingvollfjorden, where different segments of the Møre-Trøndelag Fault Complex are proposed. The new data assist in identifying the fault segments and to gain a better understanding of its subsurface expression. In total 265 new gravity stations were established in an area of 4x4 km, and 14 magnetic profiles were measured. Based on geological information, the magnetic profiles locations were chosen to cross two of the segments of MTFC and a series of anomalies can be observed in the magnetic data. A description of the instruments used in the course of the geophysical fieldwork in 2008 and the processing methods is given. Preliminary results in the form of a new gravity anomaly map and magnetic anomaly profiles are also presented. Tables of gravity observations are provided as an appendix to this report.

Keywords: Geophysical measurements	Gravity	Magnetics
Møre-Trøndelag Fault Complex	Tingvollfjorden	Eidsøra

Contents

LIST OF FIGURES

LIST OF TABLES

1. INTRODUCTION

The Møre-Trøndelag Fault Complex (MTFC) in central Norway is a long-lived structural zone whose tectonic history included dextral strike slip, sinistral strike slip, and vertical offset (Grønlie and Roberts 1989, Watts 2001). The Møre-Trøndelag Fault Complex is one of the most prominent fault zones in Norway, onshore and offshore (Gabrielsen et al. 1999). It strikes ENE-WSW, parallel to the coastline of south central Norway, and separates the northern North Sea basin system from the deep Mesozoic Møre and Vøring Basins. The Paleozoic Møre–Trøndelag Fault Complex was reactivated as a normal fault during the Mesozoic and, probably, throughout the Cenozoic until the present day. It strikes ENE-WSW, paralleling the coastline of south central Norway, and separates the northern North Sea basin system from the deep Mesozoic Møre and Vøring Basins (Redfield et al. 2005, Redfield & Osmundsen 2009) (Fig. 1).

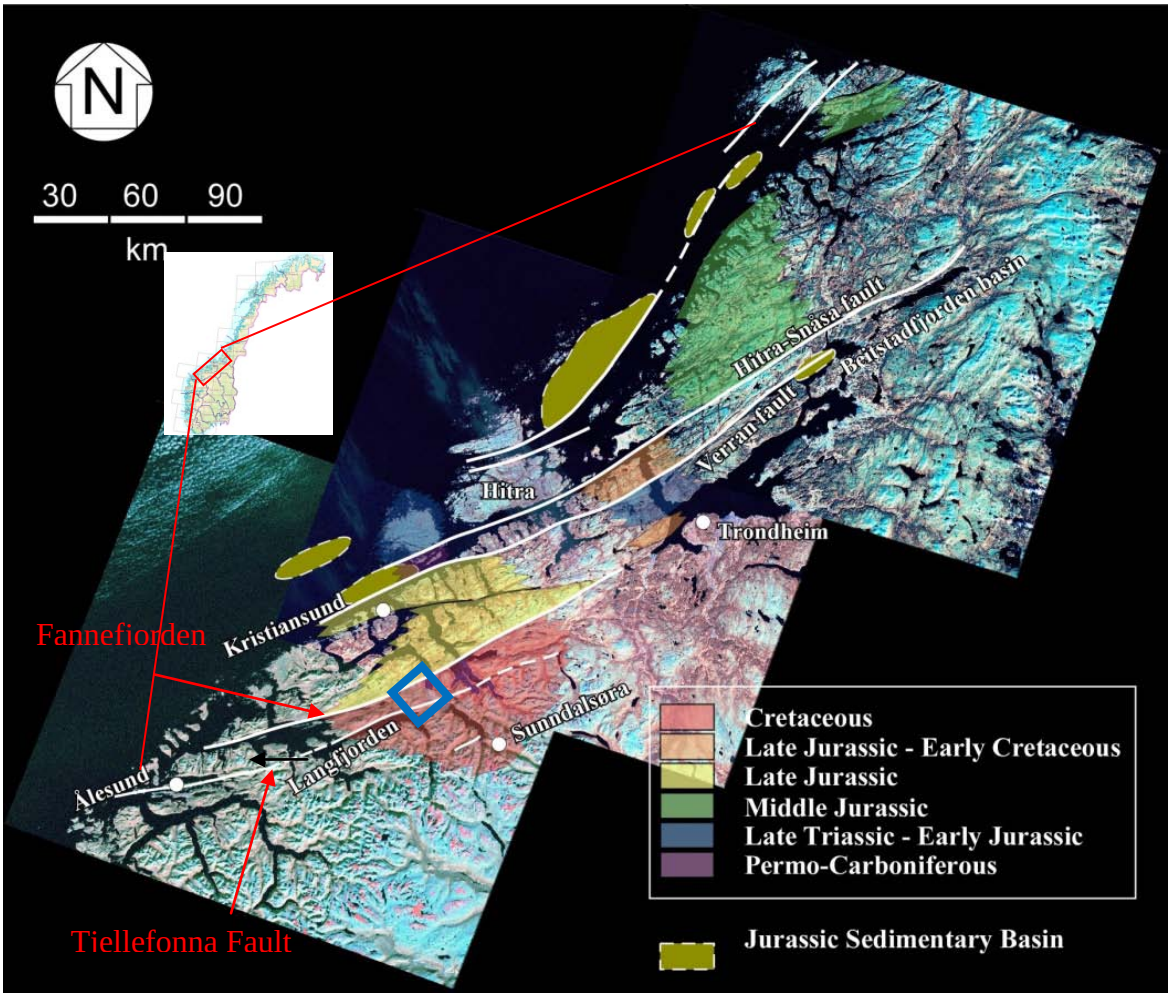

Figure 1.1 *Principal structural features of the Møre-Trøndelag Fault Complex (MTFC) and surrounding regions (modified from Redfield et al. 2005).The study area is shown with the blue box.*

Prior to this study, only regional spaced gravity data were available (Skilbrei et al. 2001; Fig. 1.2). The gravity data consist of Bouguer gravity anomaly values computed using a rock density 2670 kg/m^3. The Bouguer anomaly on land is terrain-corrected. The International Gravity Standardization Net (IGSN 71) and the Gravity Formula 1980 for normal gravity have been used to calculate the Bouguer anomalies. These data permit an interpretation of both regional and local structures. However, in order to detect the changes associated with structural offsets or fault rocks along single fault segments of the MTFC, the distance between gravity stations crossing the fault segments must be decreased.

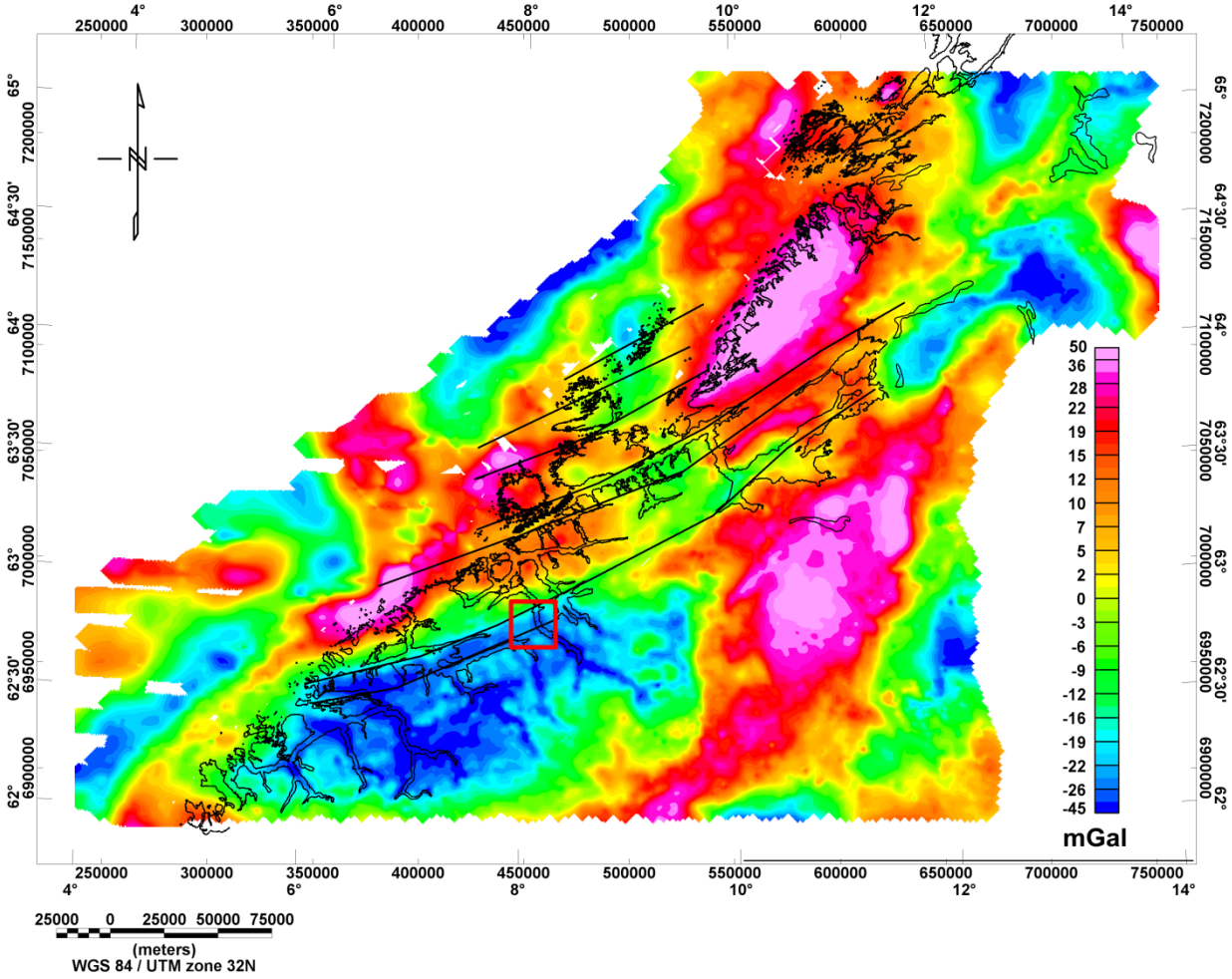

Figure 1.2 *Residual gravity anomaly produced by subtracting a third order polynomial surface from the Bouguer anomaly. The proposed segments of the MTFC are shown with black lines. The study area is depicted in red box.*

In addition an aeromagnetic data set exists, which covers the entire MTFC, but with varying resolution (Olesen et al. 2010; Fig. 1.3). The map is based on different aeromagnetic surveys with varying flight altitude, direction and line-spacing. The line spacing was smallest over mainland Norway (0.5 – 2.5 km) and largest over the continental shelf (3- 6 km). The aeromagnetic data from mainland Norway and the Norwegian continental shelf are based on a

500 × 500 m grid interpolated from digitized hand - drawn contour maps (Olesen et al. 2010). The total magnetic field was reduced by using the Definite Geomagnetic Reference Field 1965 (DGRF 1965). The flight lines are partially parallel to the fault zone, which prohibits detailed insights into the fault location and geometry.

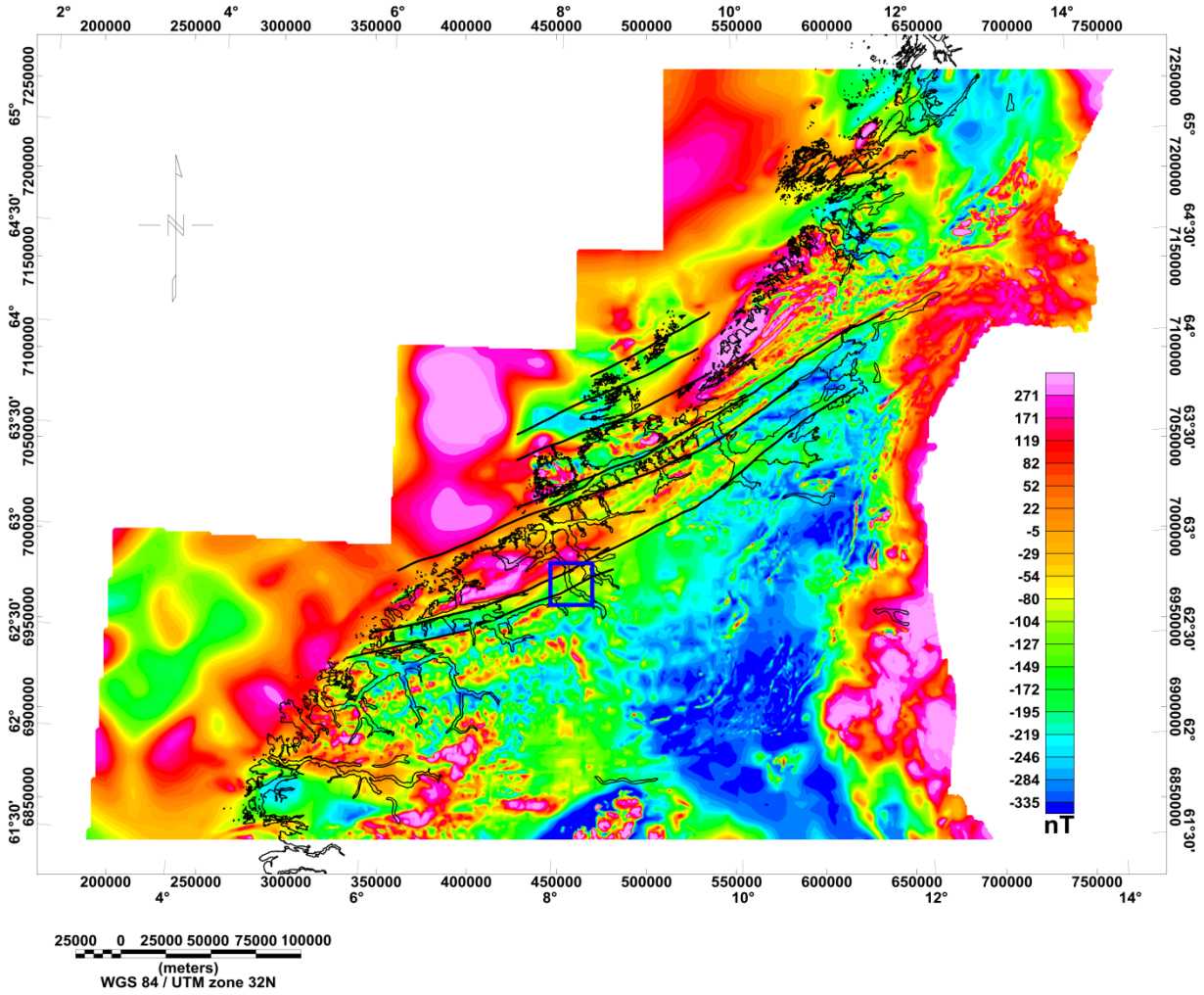

Figure 1.3 *Magnetic anomaly map. Black lines show segments of MTFC and the blue box shows the local study area.*

The measurements summarized in this report, will aid the interpretation of seismic refraction and resistivity profiles that have been already acquired in the region (Nasuti et al. 2009). Gravity and magnetic anomalies reflect changes in the physical properties of rocks at depth. Lateral changes in density and in magnetic susceptibility and remanence of rock units produce gravity and magnetic anomalies, respectively, which then will be used to create qualitative and quantitative models of the subsurface geology. The magnetic anomalies will help to trace the fault, while gravity data might furthermore help to estimate the thickness of the overburden and

to distinguish amphibolite structures, which have a distinct signal in the gravity and magnetic field, but no direct relation to segments of the Møre-Trøndelag fault Complex. The aim is to detect the faults in near subsurface by using these methods and get detailed information about the dip and exact location of the Tjellefjorden and Fannefjorden faults (Fig. 1.1).

2. DATA ACQUISTION

The geophysical data were collected by a group of 11 researchers from NTNU, the Universities of Trieste, Uppsala, Douala, Zurich and the Geological Survey of Norway (Fig. 2.1). Data acquisition was carried out from 18th to 29th of August 2008. During the field work, the group was divided into three subgroups for leveling, gravity and magnetic data acquisition, simultaneously.

Figure 2.1 *Gravity and magnetic field team*

2.1 LEVELING

Detailed information on the vertical and horizontal position of the measurements is important for the data processing. Especially for gravity, the accuracy of the elevation estimates must be in the centimeter scale to resolve Bouguer anomalies in the order of 20 microGal (μGal). Horizontal accuracy is not as crucial as vertical accuracy in the gravity processing. GPS typically provides a horizontal accuracy (<10 m) that is acceptable for gravity surveys but for

vertical positioning we used a total station survey camera with a precision of 1 mm (Figure 2.2).

Figure 2.3 shows the stations established in the study area. For the stations labeled L01 to L13 only GPS was used for estimation of the elevation and location, as these data were used for comparison and link to the available regional data. For all other stations the elevation was determined by leveling. Table 1 lists the loop closing error during leveling. In order to correct the large errors (>10 cm), we remeasured some of the loops. Nevertheless, rough topography makes some areas inaccessible and prohibited us to measure loops for all data points.

(a) **(b)**

Figure 2.2 *Leveling instruments: (a) Total station survey camera for height measurements, (b) GPSMap 60Cx used for horizontal location of the gravity points.*

Station name	Longitude	Latitude	Elevation 1 (m)	Elevation 2 (m)	Difference(m)
E01	8.10.05	62.48.05	2,270	2,229	0.05
E26	8.09.43	62.47.55	19,503	19,703	0.20
E42	8.08.50	62.47.49	43,343	43,328	0.02
F01	8.08.25	62.47.44	98,505	98,610	0.10
F09	8.08.38	62.47.43	101,173	101,131	0.04
F14	8.09.12	62.47.42	101,129	100,544	0.58
F32	8.09.48	62.47.53	79,783	79,211	0.57
F35	8.08.23	62.47.25	49,398	48,416	0.98
F133	8.08.04	62.47.44	130,667	130,620	0.05
J01	8.08.13	62.47.44	98,553	98,433	0.12

Table 1 *Loop errors and measurements for quality control of leveling. Elevation 1 and 2 show remeasurements of the station elevation. See Figure 2.3 for station location.*

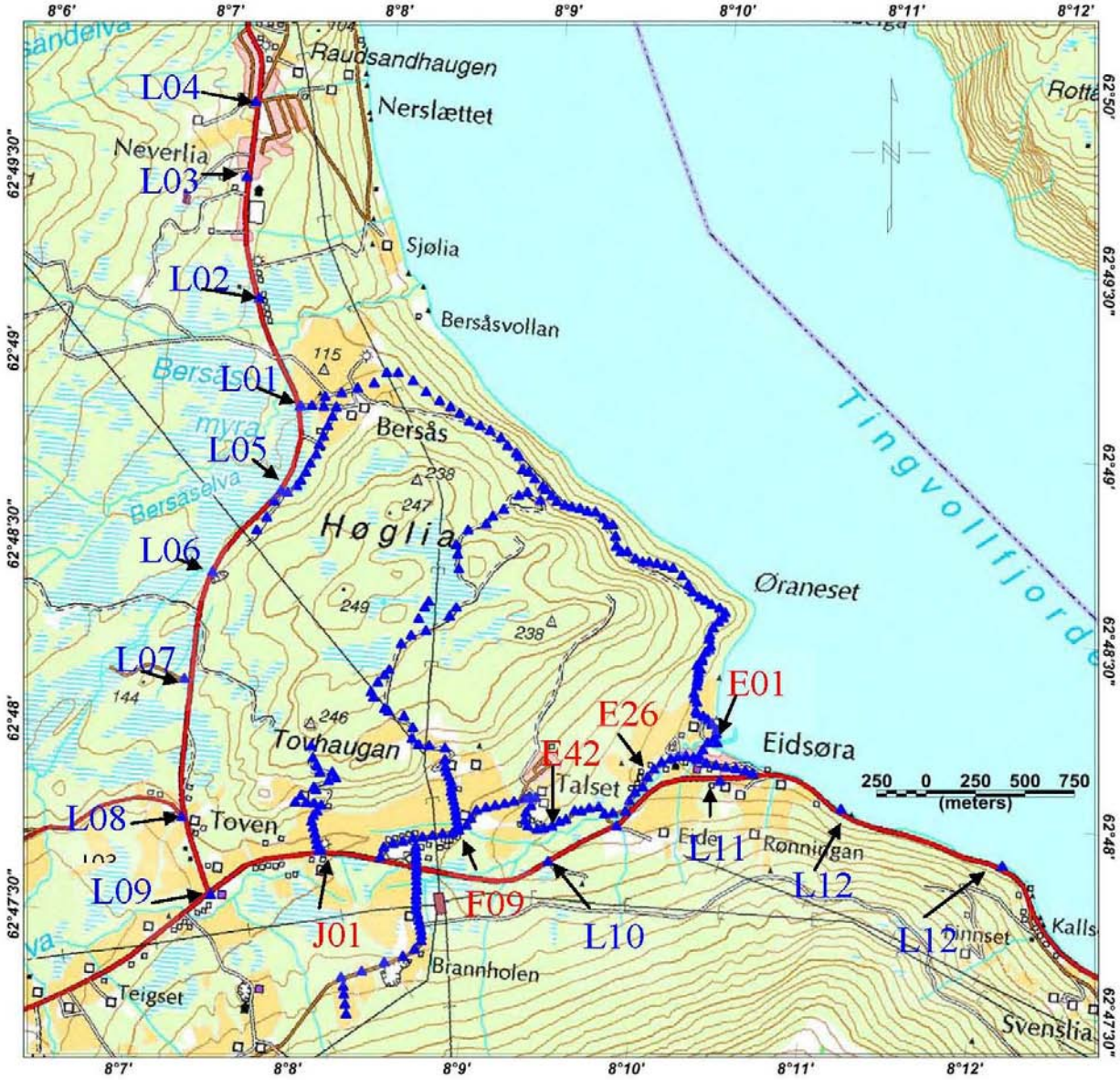

Figure 2.3 *Locations of gravity points (dark blue triangles). Stations L01 to L12 are regional gravity stations with location/height measured with GPS only. Some of stations which have been relocated and re-measured are shown with red labels.*

3. GRAVITY DATA ACQUISITION

Two gravimeters were used for the survey, the Scintrex CG-3 and the LaCoste and Romberg model G569 (Figure 3.1). The Autograv Scintrex CG-3 measures the gravity in mGal with a theoretical accuracy of 0.005 mGal. The LaCoste and Romberg model G Gravimeter (Serial No. 569), has a theoretical precision of about 0.01 mGal. Corrections are made for instrument drift by comparing repeated readings at base stations, and theoretical Earth tide corrections are made to account for the distortion of the Earth caused by the gravitational pull of the Sun and the Moon.

(a) **(b)**

Figure 3.1 *Gravimeters, (a) Scintrex CG-3, (b) Lacoste Romberg Model G*

Both gravimeters do not measure absolute gravity but measure changes in gravitational attraction from station to station. During a gravity survey, one uses a base station network, for which the values of absolute gravity are known, and links the local measurements to this network. The primary base stations used for our survey, are located in Oppdal, Molde and Sunndalsøra (Figure 3.2). These stations are part of the Norwegian Gravity Reference Network and tied to the IGSN71. The closest reference station to the survey area was in Sunndalsøra. However, due to recent rebuilding the exact location of the gravity point could not be found. Therefore, we used both the stations in Oppdal and Molde to re-establish a gravity station in Sunndalsøra and linked this point to our camp site in Trædal, near Sunndalsøra. Table 2 summarizes the information about the absolute gravity points

Readings at the base station in Trædal were taken every morning and evening on the days of measuring. A second field base station was established directly in the survey area (station

Eidsøra in Figure 3.2). Readings were repeated several times during each day of measurements.

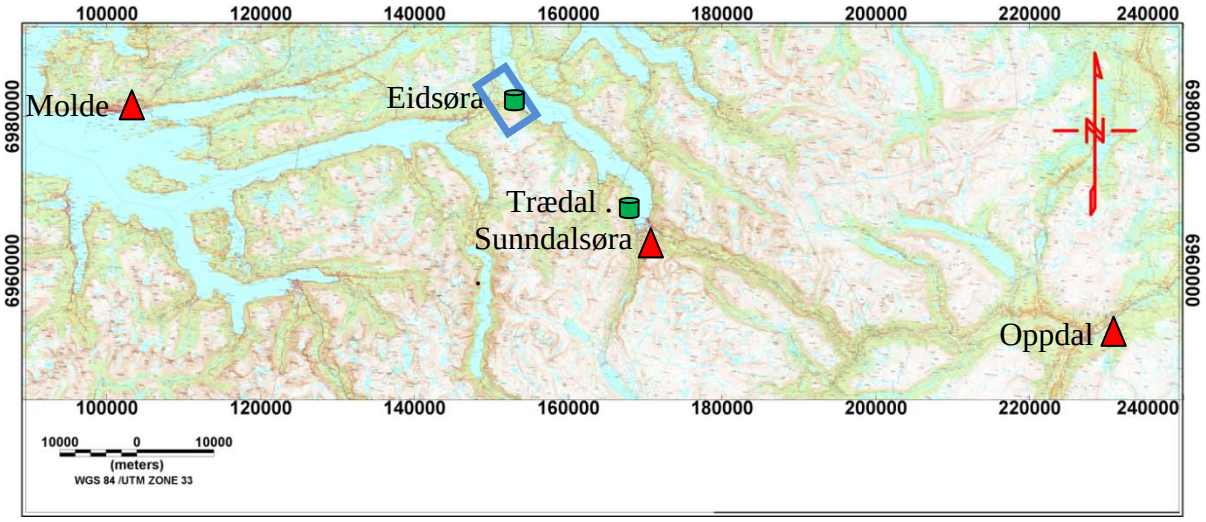

Figure 3.2 *The Norwegian Gravity Reference Network stations (red triangles) and the base station established for our gravity survey (green cylinder). The blue frame depicts the gravity survey area.*

Base name	Latitude N	Longitude W	Elevation (m)	Absolute gravity
Oppdal P	62° 35.72	9° 41.72	544,146	981950,242
Sunndalsøra	62° 40.46	8° 33.85	7,037	982034,004
Trædal	62° 39.65	8° 32.03	49,0	982028.114
Molde	62°44.30	7°09.61	5,6	982113,424

Table 2 *Gravity base stations used during data collection.*

The gravity data were collected perpendicular to the fault zone with a distance between the stations from 20 to 80 meters. In the vicinity of the faults, we reduced station spacing. For data collection the so-called 'Jump-Step method' (Figure 3.3) was used and every station was measured at least twice. This procedure is used in microgravity surveys when high accuracy is required.

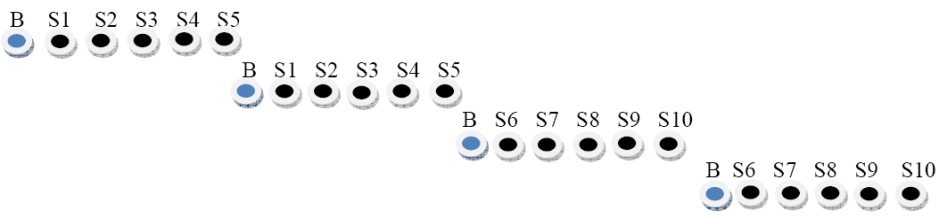

Figure 3.3 *Jump step method for gravity data acquisition. S1-S10 denote the gravity stations and B the base station.*

3.1 Gravity data processing

3.1.1 Drift correction

Together with the meter-reading from the gravimeters also date, time and station name were registered. Meter-readings are converted to observed gravity (gobs) by applying specific meter calibration constants. Then the readings are corrected for tides and the instrument drift. Earth tide corrections are calculated theoretically and account for the gravitational pull of both the sun and moon, and drift corrections remove the effects of instrument drift during the day (e.g., due to changes in pressure, battery voltage). These corrections have been applied using the DbGrav program (Institut für Geowissenschaften, CAU Kiel, Germany). The program allows correcting for the drift assuming an average curve for different reading instead of using linear correction commonly applied in other programs. An example of the drift correction is shown in Figure 3.4. The drift correction allows also evaluation of the measurements and to identify possible misreadings. In the last step, the measurements are transferred to absolute gravity measurements using the link to the base stations.

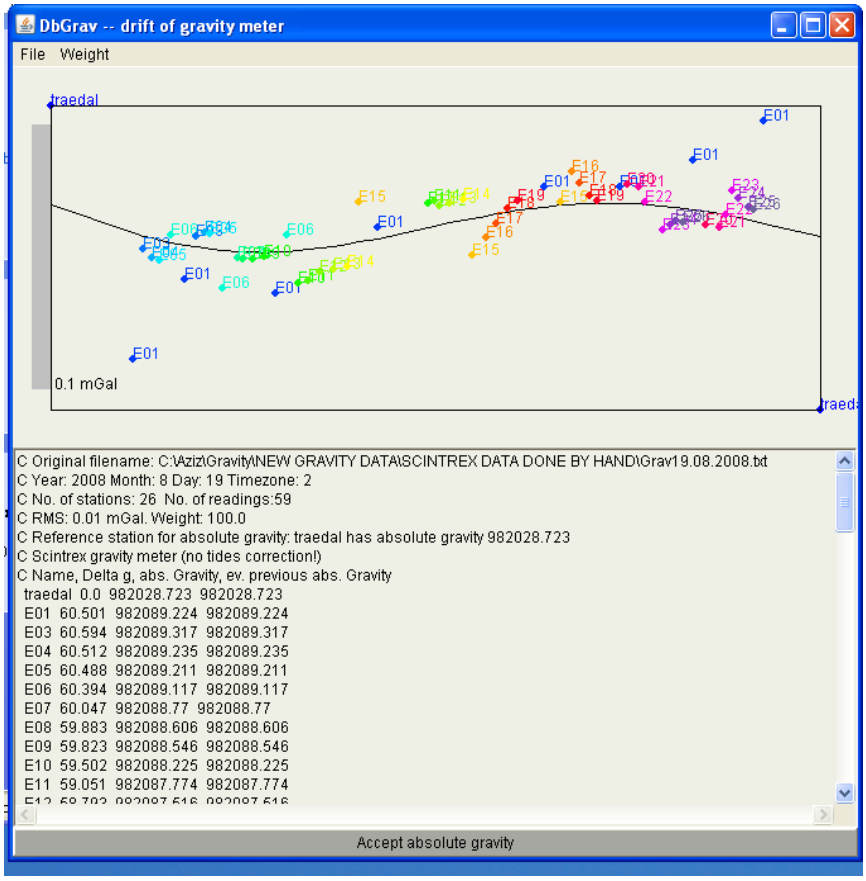

Figure 3.4 *Drift correction for the data collected on 19.08.2008 using the Dbgrav program. The base station in Trædal has been used for conversion to absolute gravity values.*

After calculating absolute gravity values, we computed gravity anomalies using Geosoft Oasis Montaj 7.1. The theoretical value of gravity accounts for gravity on the ellipsoid of a rotating Earth. We used the World Geodetic System 1984 (Blakely 1996), to calculate the normal gravity:

$$g_0 = 9.7803267714\left(\frac{1+0.00193185138639\sin^2\lambda}{\sqrt{1-0.00669437999013\sin^2\lambda}}\right) \quad (3.1)$$

where λ is the latitude of the gravity station.

3.1.2 Free-air anomaly

The free-air correction accounts for elevation of the station above the ellipsoid and assumes no mass between the station and the ellipsoid. This correction is added to the observed gravity because the increased radial distance of the station from the center of the Earth results in a lower observed gravity value than if the station were at the local datum. The free-air correction is given by

$$g_{fa} = -\frac{2g}{r}h_s \quad (3.2)$$

Where g_{fa} is free-air correction, g is absolute gravity on geoid, r is Earth's radius and h_s is station elevation. On substituting the Earth's radius (6371 km) for *r* and the mean value of gravity (981,000 mGal) for *g*, the value of g_{fa} is found to be 0.3086 mGalm^{-1}. This must be added to the measured gravity if the gravity station is above the ellipsoid and subtracted if it is below. Application of free-air correction provides the free-air anomaly given by

$$\Delta g_{fa} = g_{obs} - g_{fa} - g_0$$

Where $\Delta g_{fa}$is free-air anomaly, g_{obs} is observed gravity and $g_0$is theoretical gravity.

3.1.3 Simple Bouguer anomaly

The Bouguer correction accounts for the rock mass that is actually present between the station and the datum, and assumes an infinite horizontal slab of rock between the station and the datum. The downward pull of this slab must be subtracted from the observed gravity because the rock mass between the datum and the station exerts a downward pull on the gravimeter. The simple Bouguer correction approximates all mass above sea level with a homogeneous, infinitely extended slab of thickness equal to the height of the observation point above sea level and given by

$$g_{sb} = 2\pi\gamma\rho h_s$$

Where g_{ba} is Bouguer anomaly, γ is gravitational constant, ρ is density of the slab, and h_s is station elevation. By taking into account the simple Bouguer correction, the simple Bouguer anomaly is given by

$$\Delta g_{sb} = g_{obs} - g_{fa} - g_{sb} - g_0$$

Where Δg_{sb} is simple Bouguer anomaly, g_{obs} is observed gravity, g_{fa} is free-air correction, g_{sb} is simple Bouguer correction and g_0 is normal gravity.

3.1.4 Complete Bouguer Anomaly

The simple Bouguer correction assumes a flat slab of rock between station and datum, so if the actual topography surrounding the station is not flat, an additional correction called the terrain correction (TC) must be applied. Features such as hills, which have mass located above the station, exert a component of upward pull on the station. This causes the value of observed gravity to be less than if the topography was flat, so a correction must be added to the observed gravity at the station. Depression features such as valleys lack rock mass at the station elevation, causing measured gravity to be less than if the feature was flat. Therefore terrain corrections for depression features are also added to observed gravity.

The terrain correction was calculated using Geosoft Oasis Montaj. The gravity and terrain correction system addresses this by calculating the regional terrain correction from a coarse regional Digital Elevation Model (DEM) over a more finely sampled local DEM model that covers the survey area. This produces a regional correction grid that represents terrain correction beyond a local correction distance and this can be re-used to calculate detailed corrections at each observed gravity location. The application of all the preceding corrections results in the complete Bouguer gravity anomaly, as follows:

$$\Delta g_{cb} = \Delta g_{sb} + g_{tc}$$

Where Δg_{cb} is complete Bouguer anomaly, Δg_{sb} is Bouguer anomaly and g_{tc} is terrain correction. In additional to these corrections, a curvature correction is also applied to gravity data. This latter correction is applied to correct for the infinite horizontal slab used in the Bouguer correction. The curvature correction is based on LaFehr's formula (LaFehr 1991). By taking into account the curvature correction the complete Bouguer anomaly becomes

$$\Delta g_{cb} = \Delta g_{sb} + g_{tc} + g_{curv}$$

with g_{curv} the curvature correction. Figure 3.5 shows the Bouguer anomaly values for the measured points using a Bouguer reduction density of 2790 kg/m^3 (see below for choice of value).

3.1.5 Density determination for Bouguer correction

Rock densities can be determined by actually measuring samples. However, densities usually vary over a wide range even within the same rock formation, so that a large number of samples is required for a reliable average value. Also, it is often difficult to get samples which are far enough below the weathered surface to be typical of the rock material within the range of the topography. Therefore, we applied the well-known Nettleton method (Nettleton 1939) to estimate the 'best' density for Bouguer correction.

The density is estimated by simply plotting the gravity values across a topographic feature, and finding the density value for which the reduced curve has a minimum correlation with the topography by reduction with different density values. The sample is an entire topographic unit and the value obtained is the average density of all material within the elevation range of the gravity traverse. It is essential that the topographic feature selected for a density profile should have at least one reversal. A hill is preferable to a valley because the density is more apt to be uniform and typical of the topography as a whole, as valleys frequently contain alluvial material, the density of which is different from that of the general rock section (Nettleton 1939). Figure 3.5 shows the Bouguer anomaly by using density 2790 kg/m^3. A gravity map has been produced by gridding these data (Figure 3.6). The optimum density is obtained along the traverse (A-B, Figures 3.5). The result of using different densities is shown in Figure 3.7.

The new gravity map shows no pronounced difference between maximum and minimum gravity anomalies (< 2 mGal). The anomalies follow roughly the topographic variations. In the valley we have more negative anomalies than other places(Figure 3.6), which may reflect the overburden which varies in thickness from 1 meter to 20 meters in the valley (Nasuti et al. 2009).

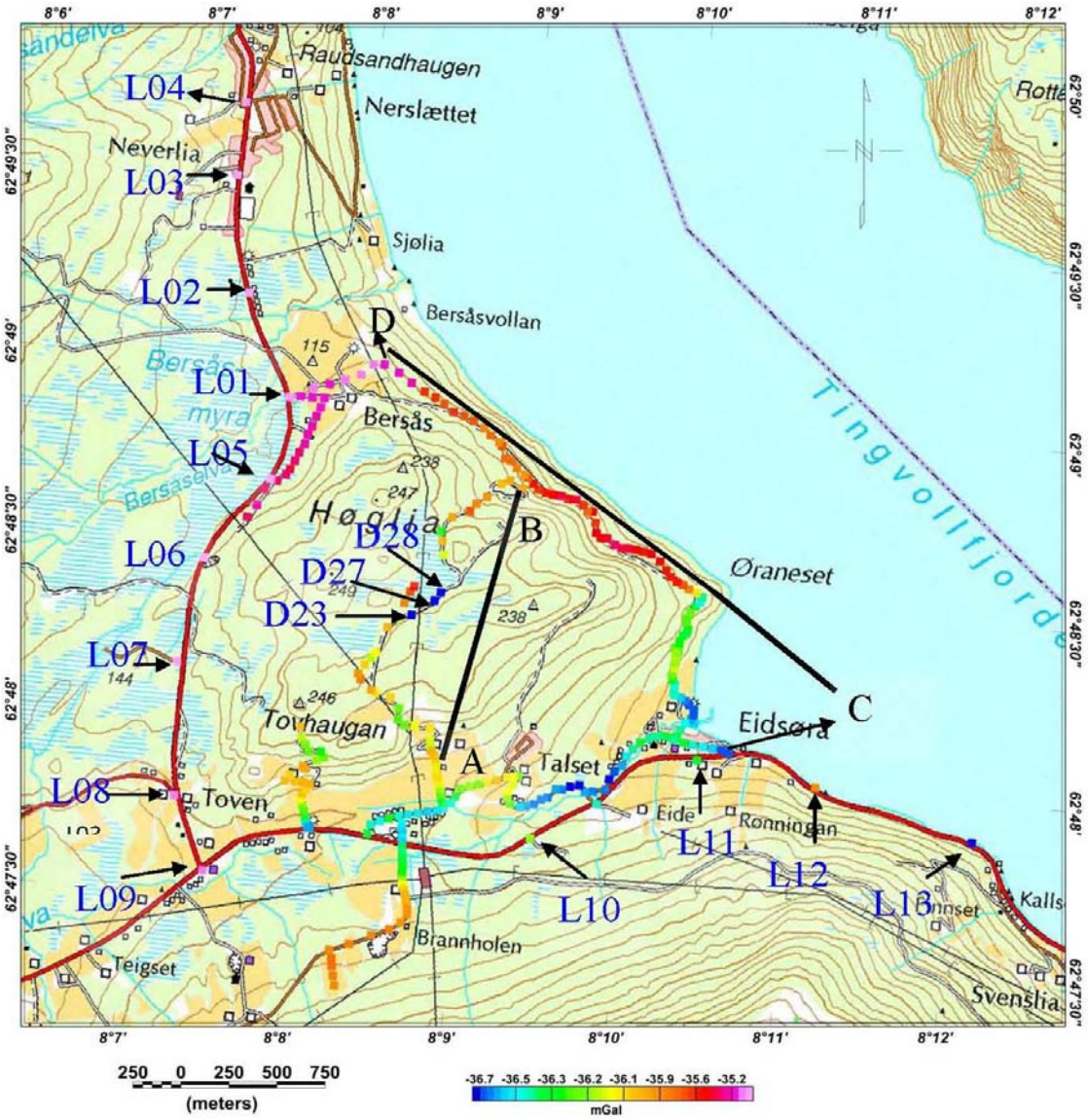

Figure 3.5 *Complete Bouguer anomaly for station by using a density of 2790 kg/m^{3}for Bouguer slab density. L01- L13 show the regional gravity stations. AB indicates the traverse used for the Nettleton method (Fig. 3.7). CD shows a profile extracted from gravity points shown in Figure 3.8. Stations L01 to L013 have been measured using the LaCoste Romberg gravimeter and GPS-positioning. These stations have been collected for regional-scale modeling. Stations D27, D23 and D28 present significantly different gravity values with as compared with the other stations in the neighborhood. These values could result from a local geological structure or from data errors.*

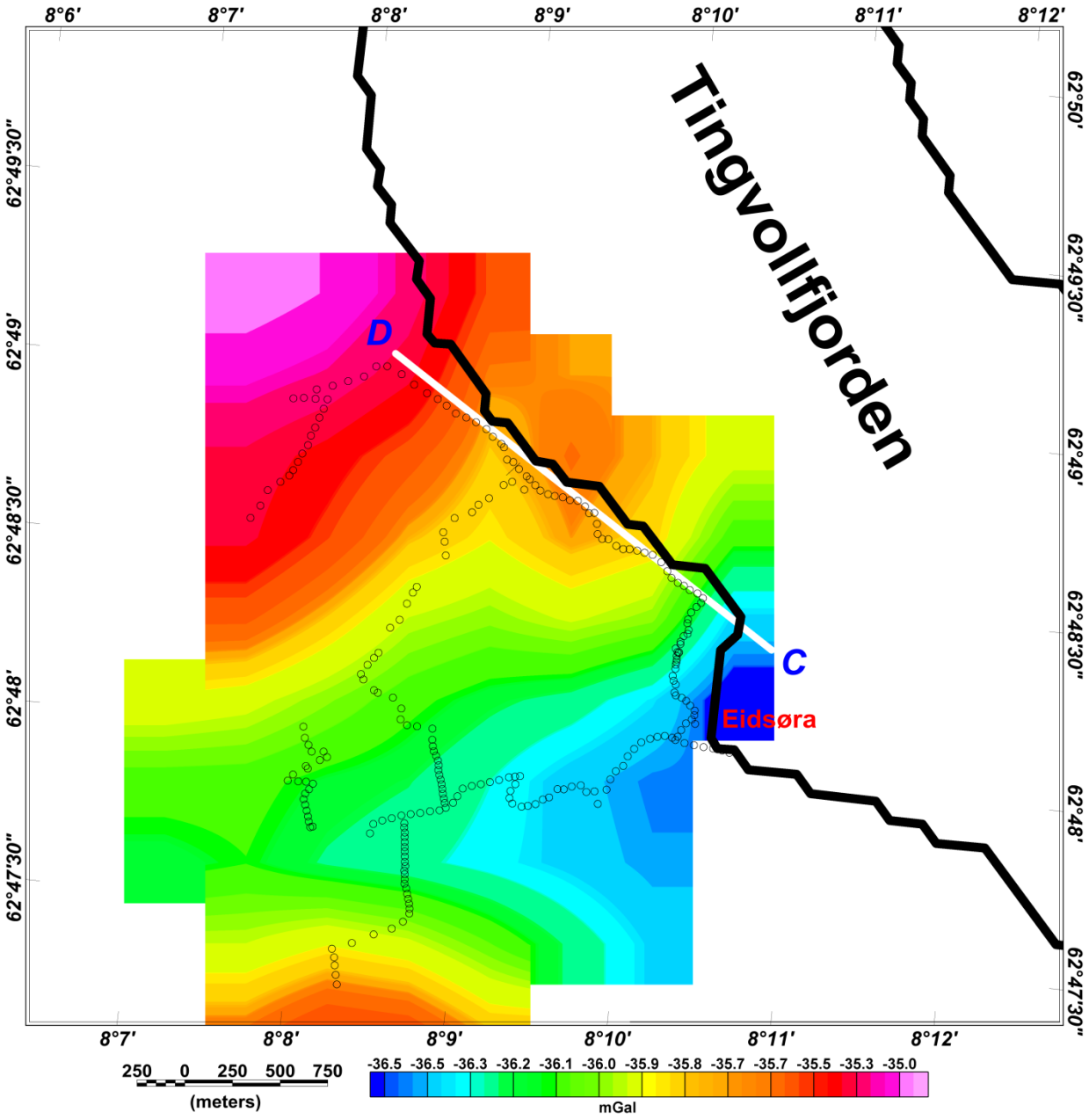

Figure 3.6 *Complete Bouguer anomaly map by using a density of 2790 kg/m^{3}for Bouguer slab density. A cell size of 500 by 500 m is used for gridding. The gravity stations are shown in small circles. CD shows a profile extracted from gravity points shown in Figure 3.7.*

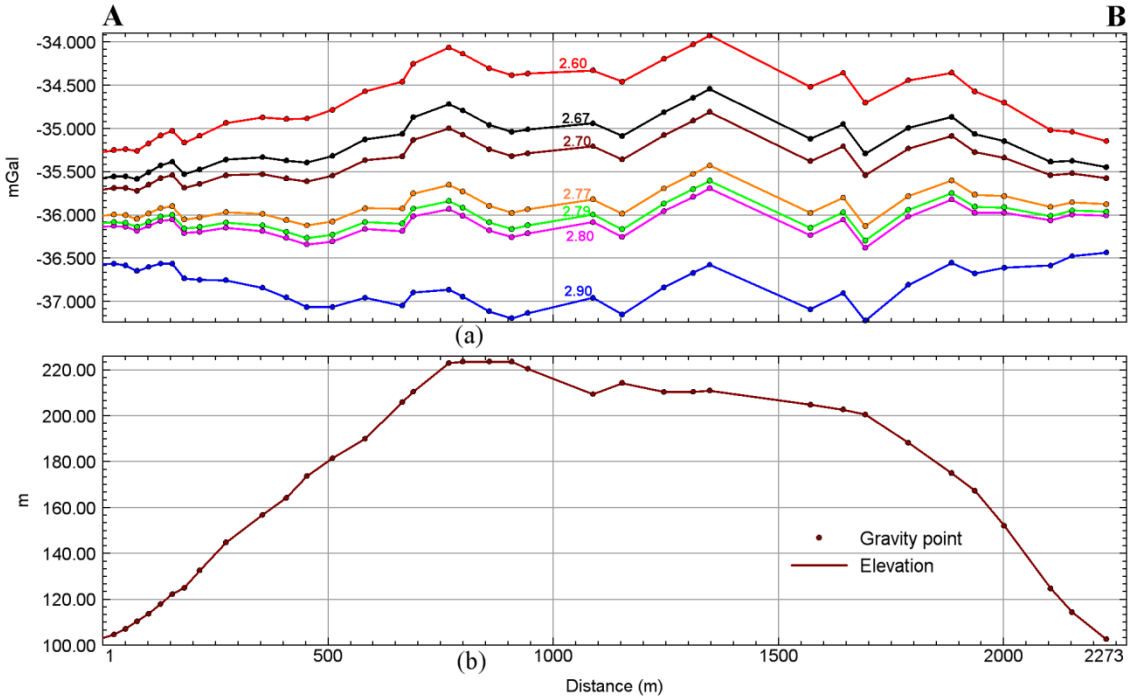

Figure 3.7 *Determination of density using Nettleton method. (a) Gravity profile (A-B) for various densities (in g/cm^3). (b) Topography of the profile with the location of gravity stations. See Figure 3.5 for profile location.*

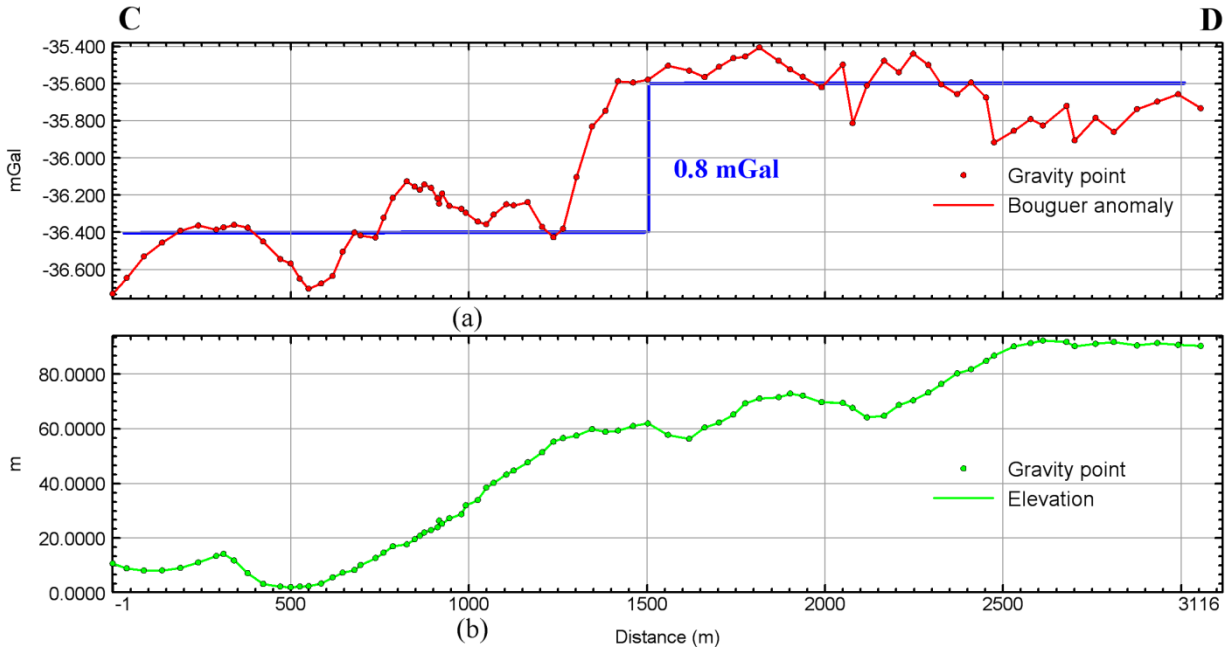

Figure 3.8 *Gravity profile (C-D). (a) Bouguer gravity, blue line indicates a step in the gravity data. (b) Elevation of gravity points. See Figure 3.5 for profile location.*

4. MAGNETIC DATA ACQUISITION

Magnetic data have been acquired along a series of profiles crossing two segments of the MTFC (Fig. 4.1). In total, fifteen profiles were measured: Profiles 1 to 8 are located across the proposed location of the Tjellefjonna fault and Profiles 10 to 15 across the Fannefjorden fault. Profile 9 is located in between the two segments to study the existence of possible minor faults related to the larger segments (Fig. 4.1). The measurements were conducted using an advanced GEM magnetometer GSM-19 with two sensors separated vertically by 56 cm in order to measure vertical gradients and the total magnetic field simultaneously (Fig. 4.2). The magnetometer records the magnetic field and gradient in different modes. We used Walkgrad mode to measure vertical gradient and magnetic field continuously. The rate of the measurement is 5 measurements per second. To correct for the effect of diurnal variations a second magnetometer was deployed in the area. The base magnetometer was located close to the survey area. We used a Sintrex ENVI-MAG magnetometer and set up it to record the magnetic field every 5 seconds continuously during the day (Fig. 4.3). Two locations for the base stations were used (Figure 4.1). Base 2 was used for Profile 9 only. The coordinates of the base stations are shown in Table 2.

4.1 Magnetic data processing

A significant number of power lines and different infrastructures (pipes, houses, etc.) exist in the survey area. Therefore, relatively high noise levels were recorded along some of the profiles. Such high-amplitude noise overprints the anomalies related to geological structures and must be removed before processing. During the measurements the location of the infrastructures was noted (Table 3), but additional structures in the subsurface (e.g., pipelines) could exist. Cultural noise sources such as barbed-wire fences were also noted. Some parts of the profiles had to be completely disregarded due to a high-noise level. The magnetic data were further corrected for diurnal variations using the base station readings, and the International Geomagnetic Reference Field 2005 (IGRF 2005) was removed.

Because of the various infrastructures and the rugged ground surface, the vertical gradient is for most of the profiles too noisy. To remove this effect a low-pass filter has been used. However, in some profiles like Profile 2, the vertical gradient is still noisy. Application of a stronger filter may diminish all relevant geological signal.

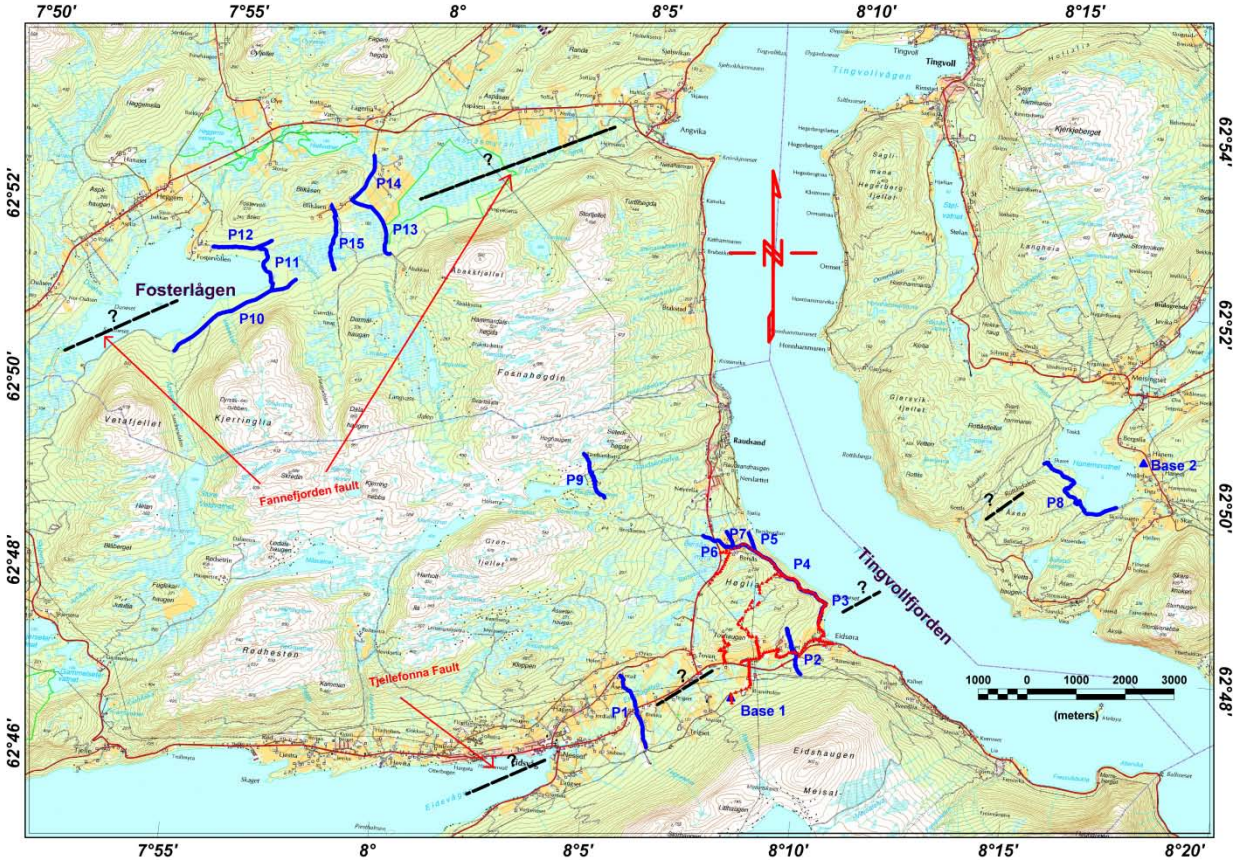

Figure 4.1 *Gravity and magnetic surveys depicted as red dots and blue lines, respectively. Base stations for magnetic measurement are indicated with blue triangles. The proposed segments of the MTFC, Tjellefonna and Fannefjorden faults, are shown with the dashed, black line.*

Figure 4.2 *GEM magnetometer GSM-19 V used here as portable magnetometer.*

Figure 4.3 Sintrex *ENVI-MAG magnetometer used here as base magnetometer.*

Base Station	Longitude	Latitude
Base 1	08.08.17	62.47.21
Base 2	08.17.32	62.50.23

Table 3 *Base stations used for the magnetic survey*

Profile	X (Degree)	Y (Degree)	Descriptions
L.1	8.06.03	62.47.07	Buildings
L.1	8.05.39	62.47.26	Buildings
L.1	8.05.36	62.47.27	Buildings
L.1	8.05.33	62.47.27	Buildings and power lines
L.1	8.05.27	62.47.27	Road and some pipe lines
L.2	8.09.44	62.47.47	Electric fence
L.2	8.09.43	62.47.48	Road and power line
L.2	8.09.43	62.47.54	Road and power line
L.3	8.10.13	62.48.26	Pipe line
L.3	8.10.12	62.48.22	Pipe line
L.3	8.10.12	62.48.20	Pipe line
L. 3	8.10.11	62.48.19	Pipe line
L.3	8.10.17	62.48.28	Pipe line
L.3	8.10.13	62.48.26	Pipe line
L.6	8.08.09	62.49.02	Strong power line
L.6	8.07.32	62.49.03	Metallic bridge
L.8	8.15.34	62.50.11	Agricultural equipments
L.10	7.54.07	62.50.28	Bridge-this part is removed
L.10	7.55.04	62.50.55	Pipe line
L.10	7.55.11	62.50.57	Pipe line
L.12	7.54.46	62.51.39	Buildings-this part is removed
L.13	7.58.50	62.52.02	Power line
L.13	7.58.23	62.52.17	Power line
L.13	7.58.52	62.51.49	Parking place
L.14	7.58.23	62.52.39	Power line
L.14	7.58.00	62.52.22	Power line

Table 4 *Locations of power lines and other kind of infrastructures*

4.2 Magnetic results

Diurnal correction, reduced magnetic data and the vertical gradient of the total magnetic field are presented for the individual profiles in Figures 4.4 to 4.17. The diurnal correction for all the profile are less than 15 nT which means that the survey has been carried out under relatively quiet magnetic conditions. In the reminder we present the profiles and discuss the most significant anomalies.

4.2.1 Profile 1

This profile is conducted to cross the suspected fault zone (Tjellefonna fault) perpendicularly. Because of the presence of power lines and other kinds of infrastructures we skipped measurements along sections (1) and (3) (Fig. 4.4b). Number (2) indicates a low magnetic anomaly with a short wavelength probably related to a powerline. Figure 4.4c shows the vertical gradient. Numbers (1) and (3) outline the skipped sections. Anomaly number (2) is probably the effect of a power line and anomaly number (4) is related to some near-surface infrastructure. No anomaly could be clearly related to a fault segment.

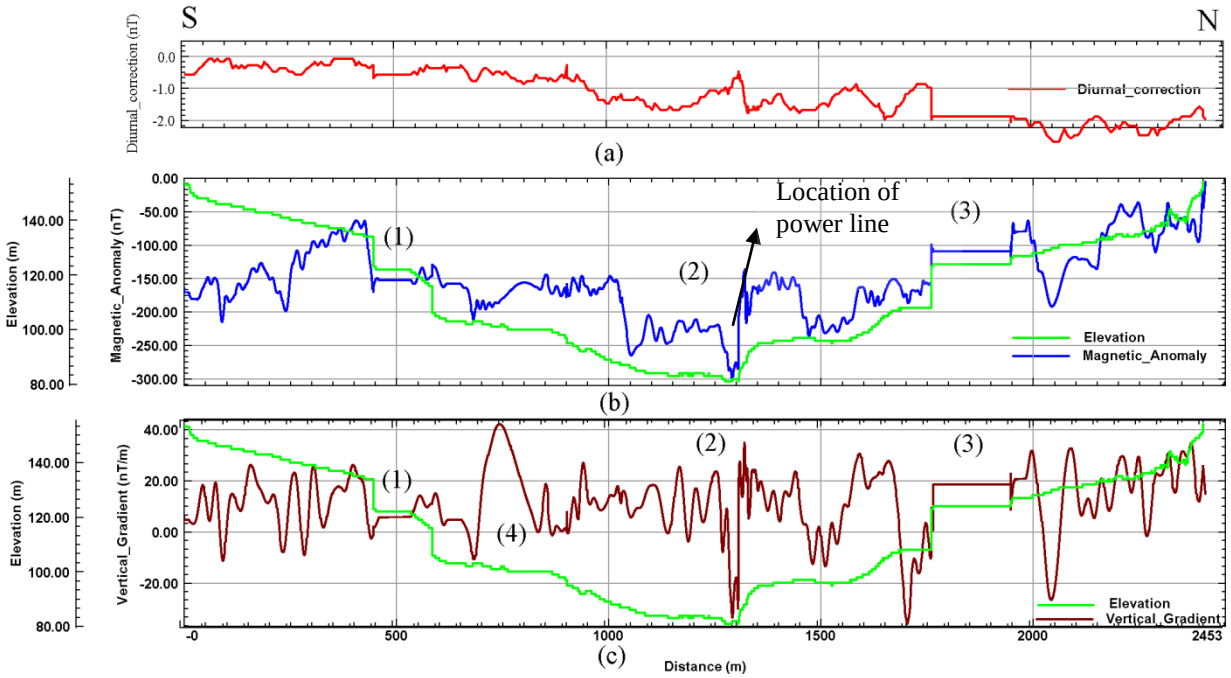

Figure 4.4 *Magnetic Profile 8, (a) Diurnal corrections for the measurements, (b) magnetic anomaly and (c) vertical gradient of the total magnetic field.*

4.2.2 Profile 2

This profile is almost 1500 meter long and located ~2 km west of Eidsøra. The profile crosses through a densely forested valley. We expected to cross the fault perpendicularly. Magnetic anomalies are shown in Figure 4.5b. Due to field conditions very high frequency signals were recorded. In order to remove the high frequency noise (short wavelength) a low-pass filter was applied to the recorded magnetic anomalies (Fig. 4.5c). Afterwards, an anomaly with amplitude of 80 nT can be clearly distinguished (number (1) in Figure 4.5c). This anomaly is probably related to brittle structures present in the bedrock. A section numbered (2) represents a part of the profile which has been skipped because of a road crossing. The vertical gradient appears to be relatively noisy (Fig. 4.5d). The reason for this is the rugged topographic path followed by the operator across the forest and implying inevitable changes in magnetometer height.

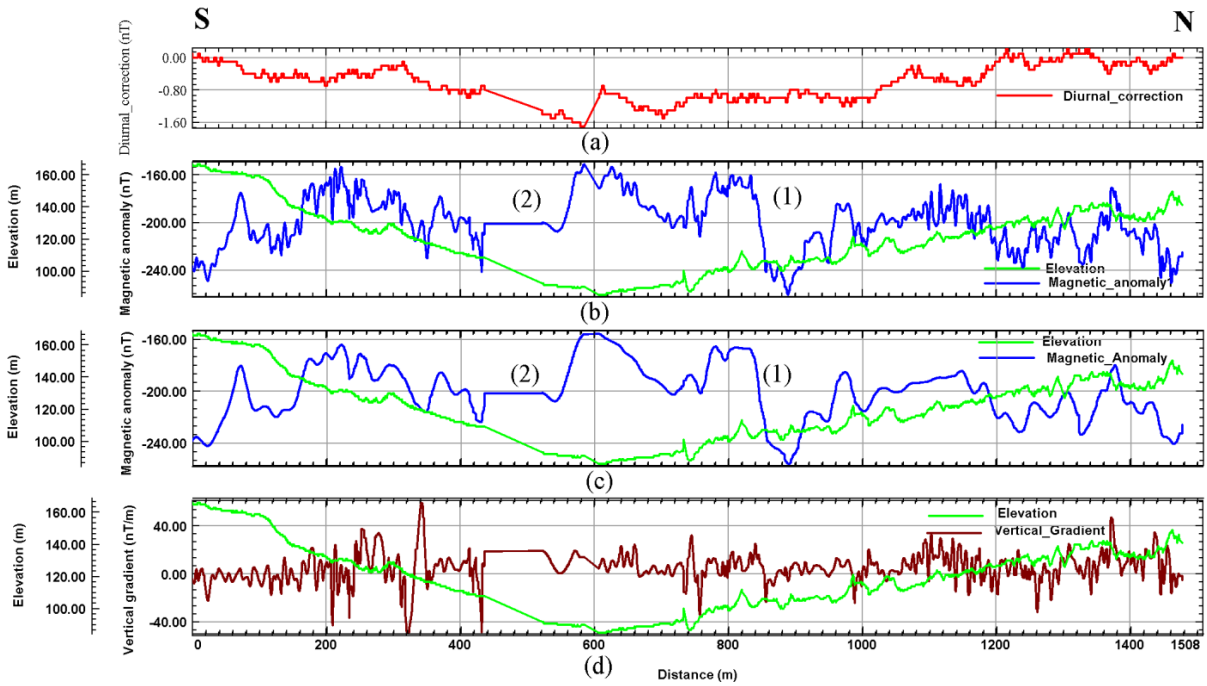

Figure 4.5 *Magnetic profile 7, (a) Diurnal corrections, (b) magnetic anomaly (c), filtered magnetic anomaly and (d) vertical gradient of the total magnetic field.*

4.2.3 Profile 3

This profile is ~840 meter long and located near Eidsøra. Some pronounced magnetic anomalies were detected ((1), (2), (3) and (4) in Figure 4.6b). NE of anomaly (3), magnetic values increase gradually whereas SW of it they remain relatively constant. The vertical gradient shows the same anomalies as the total magnetic field represented in Figure 4.6b.

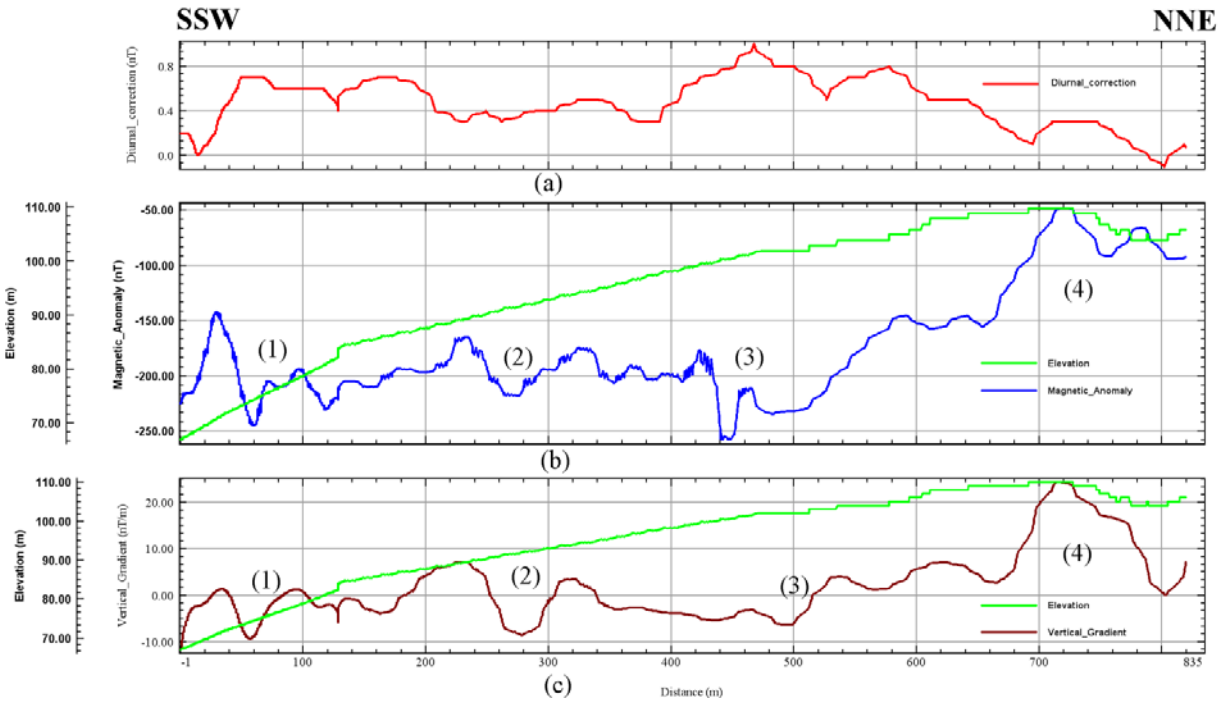

Figure 4.6 *Magnetic Profile 3, (a) Diurnal corrections, (b) magnetic anomaly and (c) vertical gradient of the total magnetic field.*

4.2.4 Profile 4

This profile is almost 1800 m long and is located near Eidsøra. A very high-amplitude magnetic anomaly of 1500 nT is seen along this profile (Figure 4.7b). This anomaly is probably related to the presence of an amphibolite body. An outcrop of this highly magnetic body has been detected along this profile. A similar anomaly but with smaller amplitude is also seen on the vertical gradient of magnetic field (Fig. 4.7c).

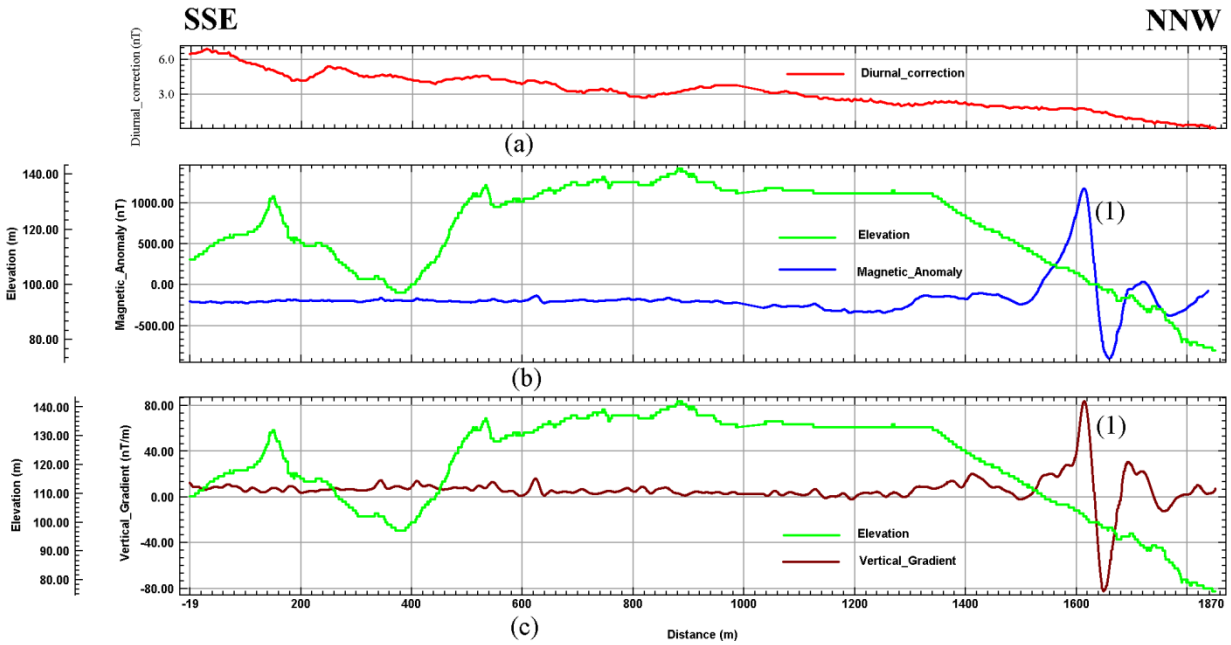

Figure 4.7 *Magnetic Profile 4, (a) Diurnal corrections, (b) magnetic anomaly and (c) vertical gradient of the total magnetic field.*

4.2.5 Profile 5

This profile is 400 meter long. As shown in Figure 4.1 the profile overlaps partly Profile 4. The aim here was to focus on the high amplitude magnetic body (Fig. 4.8). This anomaly is located in the middle of the profile and very pronounced with amplitude of 1500 nT. This anomaly could be caused by a magnetite rich body. The magnetic values adjacent to the anomaly are similar, which points to a homogeneous geological background. In addition, the shape of the anomaly resembles very much the ones commonly associated to magnetized dykes.

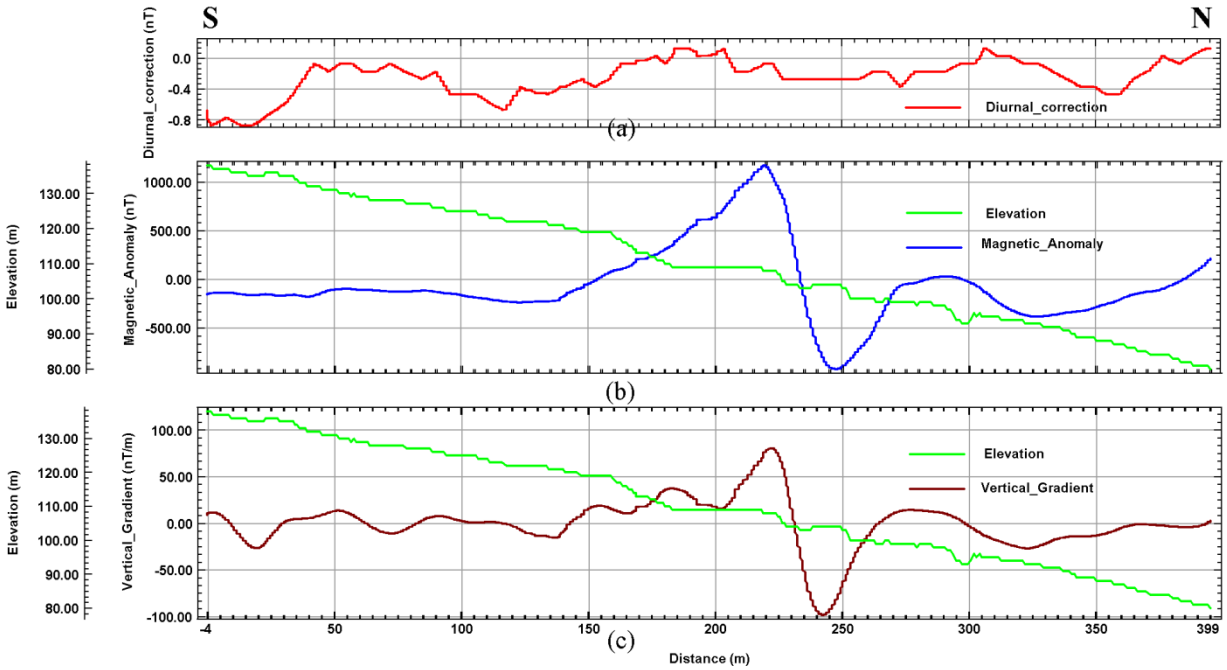

Figure 4.8 *Magnetic Profile 5, (a) Diurnal corrections, (b) magnetic anomaly and (c) vertical gradient of the total magnetic field.*

4.2.6 Profile 6

This profile starts at the southern end of Profile 4 (Fig. 4.1). Diurnal variations in the Earth's magnetic field were negligible during the recording time (Fig. 4.9a). Four distinct anomalies can be detected. A very high amplitude magnetic anomaly number (2) with a symmetric shape is shown in Fig. 4.9b. This anomaly is probably related to the same structure which has already been mentioned for Profiles 4 and 5 but here it has a symmetric shape. There are some other magnetic anomalies labeled (1), (3) and (4) in Fig. 4.9b. Vertical gradient values remain positive all along the profile which emphasis the symmetric anomalies. All magnetic anomalies except anomaly (1) find their counterparts in the variations of the vertical gradient.

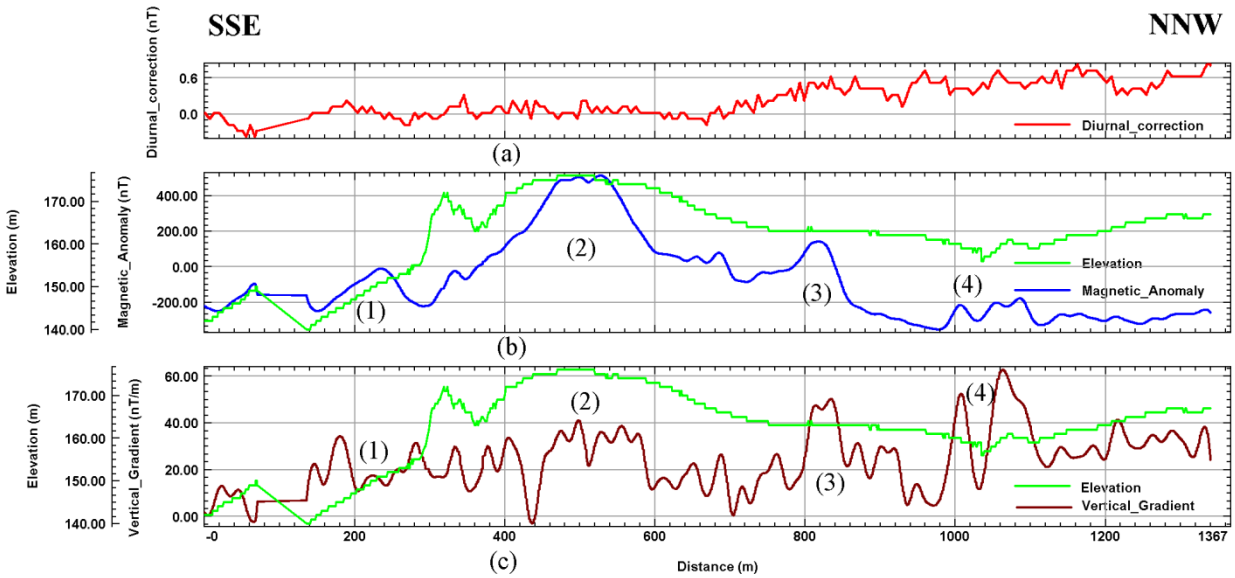

Figure 4.9 *Magnetic Profile 6, (a) Diurnal corrections, (b) magnetic anomaly and (c) vertical gradient of the total magnetic field.*

4.2.7 Profile 7

This profile was conducted parallel to Profile 5 (Fig. 4.1). Figure 4.10 shows several magnetic anomalies. By comparing the variations in magnetic values and topography we clearly see that the magnetic trend from anomaly number (1) to (3) is influenced by the topography. The vertical gradient shows similar anomalies (Fig. 4.10c).

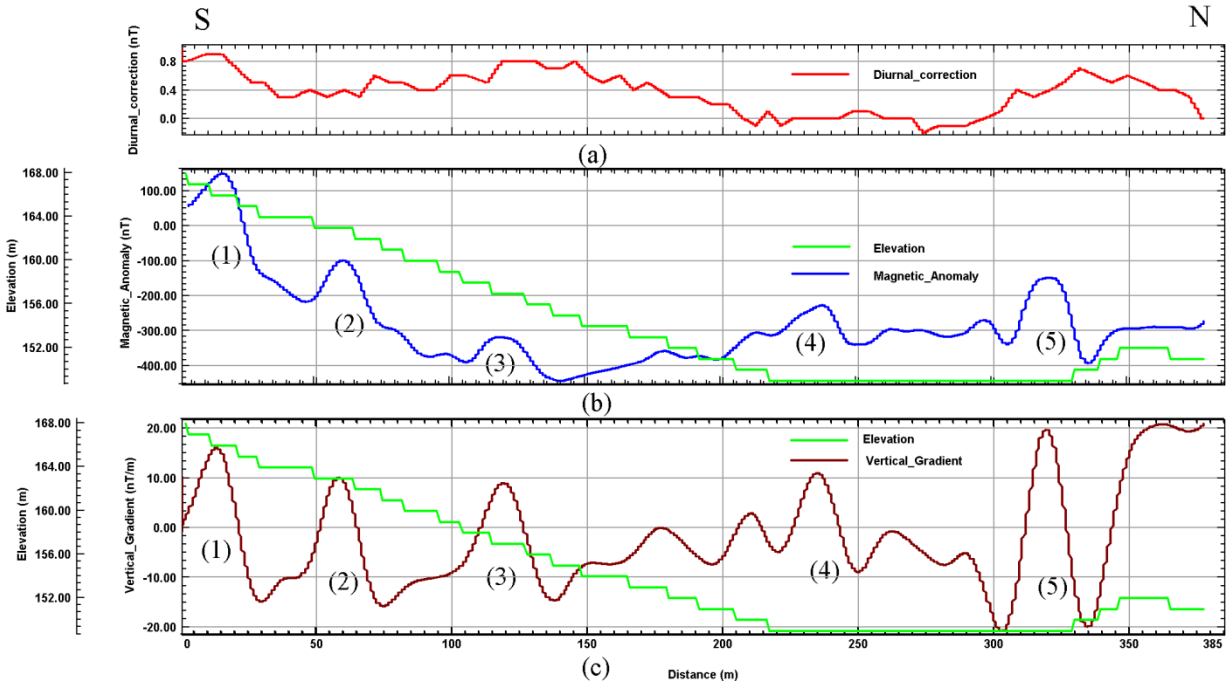

Figure 4.10 *Magnetic profile 7, (a) Diurnal corrections, (b) magnetic anomaly and (c) vertical gradient of the total magnetic field.*

4.2.8 Profile 8

This profile is located on the eastern side of Tingvollfjorden (Fig. 4.1). The magnetic signal along this specific profile is used to constrain interpretations derived from other geophysical methods like resistivity and seismics. Diurnal variations of the magnetic field are less than 12 nT (Fig. 4.11a). Two pronounced anomalies are seen in Figure 4.11b. Anomaly number (1) shows a step in the magnetic field where the higher value in the southern part is well isolated. Anomaly number (2) is expressed as a depression. The vertical gradient along the present profile is very noisy (Figure 4.11c) and this casts some doubts on the significance of the pronounced anomaly seen close to the southern end of the profile. Anomaly number (1) is due to technical problems while recording data and does not reflect a geological anomaly.

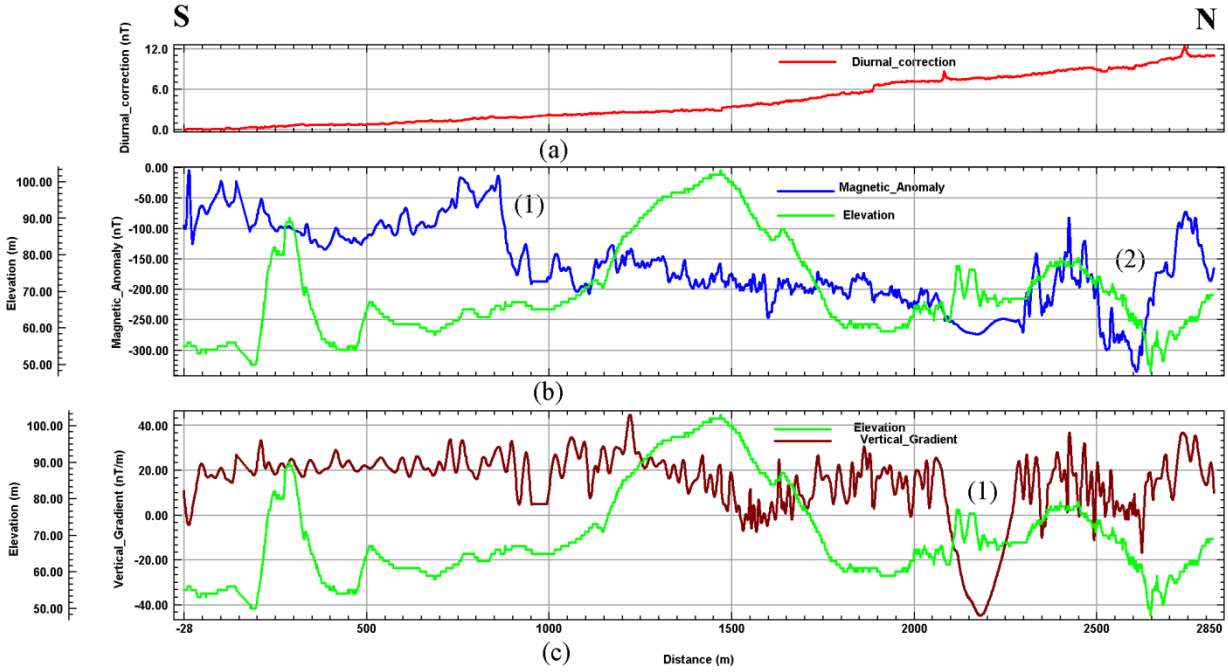

Figure 4.11 *Magnetic Profile 8,(a) Diurnal corrections, (b) magnetic anomaly and (c) vertical gradient of the total magnetic field.*

4.2.9 Profile 9

This profile is located at a relatively high elevation (i.e. 400-500 m a.s.l., Fig. 4.1). Diurnal variations for the Earth magnetic field during the measurements were in the order of 5 nT (Fig. 4.12a). A very distinctive anomaly is observed at the beginning of the profile (No. 1, Fig.4.12b) with an amplitude of almost 400 nT. There are also some other modest anomalies. Figure 4.12c shows the vertical gradient of the magnetic field where we can observe the same anomalies as in the magnetic total field. The source of these anomalies is probably located in the shallow subsurface as the anomalies show high amplitudes and short wavelengths.

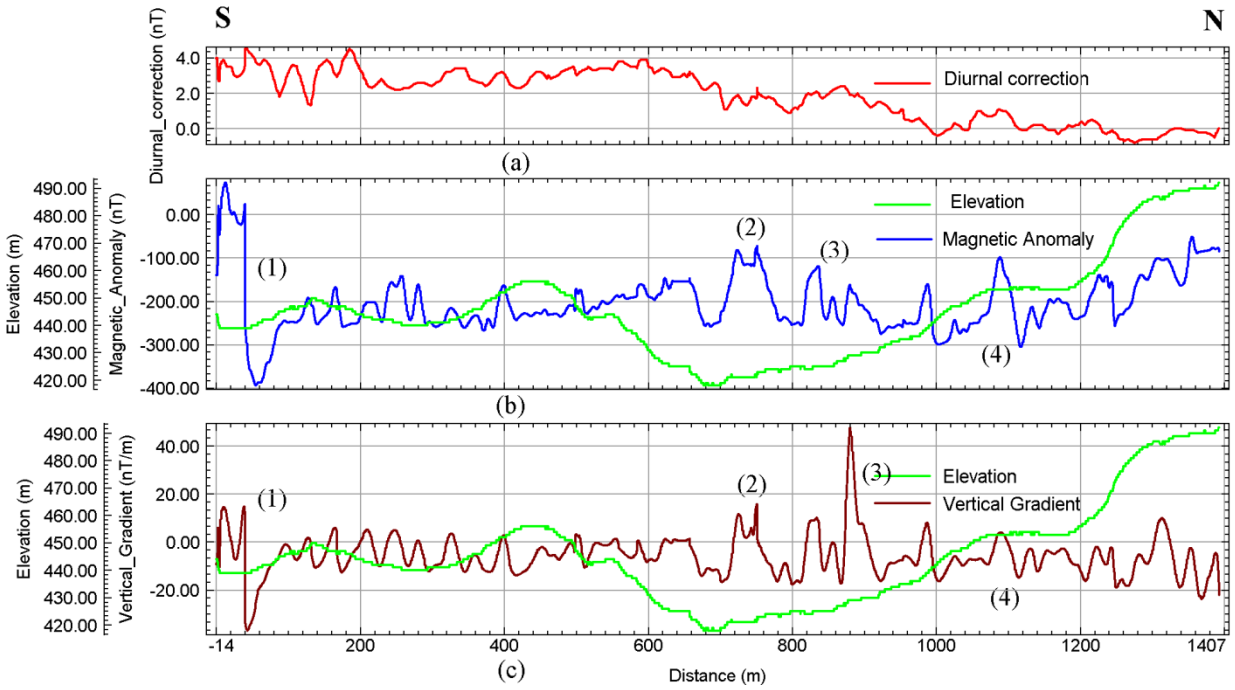

Figure 4.12 *Magnetic Profile 9. (a) Diurnal corrections, (b) magnetic anomalies and (c) vertical gradients of the total magnetic field.*

4.2.10 Profile 10

This profile is almost 3 km long and is located on the southern shore of the Fosterlågen Lake (Fig. 4.13). This profile is following a road with very gentle topography. Three anomalies are depicted in Fig. 4.13b. Although the vertical gradient appears to be very noisy, we could isolate two distinct anomalies which are numbered (1) and (2). Gradient anomaly number (2) finds its counterpart in the magnetic anomalies in contrast to anomaly number (1), which is probably related to a shallow source body.

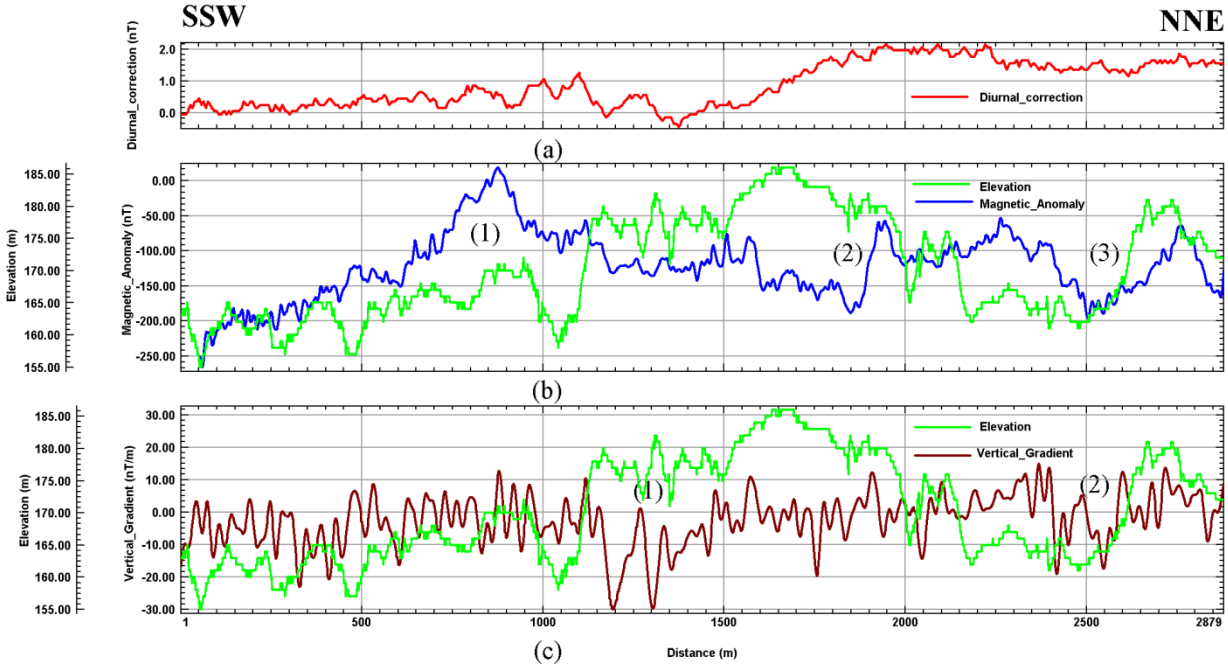

Figure 4.13 *Magnetic Profile 10, (a) Diurnal corrections, (b) magnetic anomaly and (c) vertical gradient of the total magnetic field.*

4.2.11 Profile 11

This profile strikes almost N-S (Fig. 4.14) and is located on the eastern shore of the Fosterlågen Lake. The location of the profile should cross the Fannefjorden fault perpendicularly. A low magnetic anomaly can be isolated with some smaller anomalies nearby ((1) in Fig. 4.14b). This profile shows an increase after distance 800 m to the northern end. In the vertical gradient profile an anomaly with amplitude 80nT/m is distinguished which has its counterpart in the magnetic anomaly. The width of the anomaly indicates a shallow source location (Figure 4.14c).

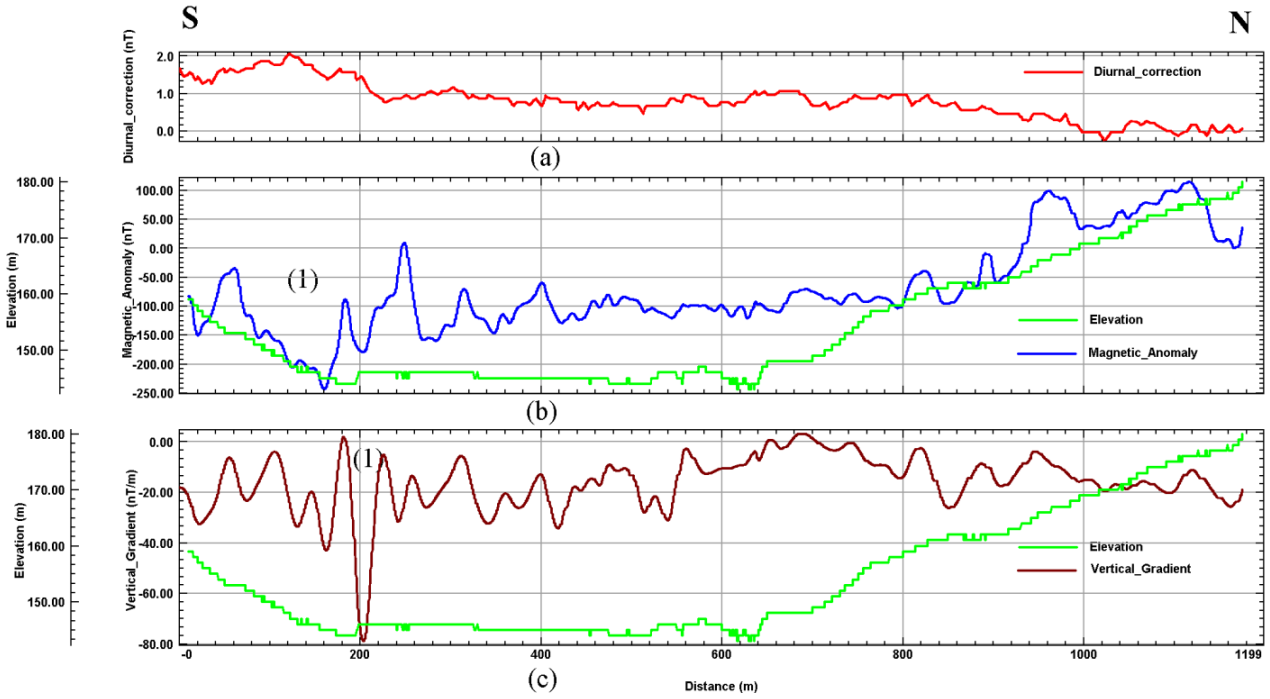

Figure 4.14 *Magnetic Profile 11, (a) Diurnal corrections, (b) magnetic anomaly and (c) vertical gradient of the total magnetic field.*

4.2.12 Profile 12

This profile strikes W-E and is located northeast of Fosterlågen Lake (Fig. 4.1). An anomaly of ~400 nT is seen in Figure 4.15b (i.e. number (1)). The vertical gradient (Fig. 4.15c) shows various anomalies. Three high amplitude anomalies correlate with the magnetic anomalies isolated in Figure 4.15b. Anomaly numbered (3) shows a very short wave-length and probably is related to a very shallow or non-geologic structure.

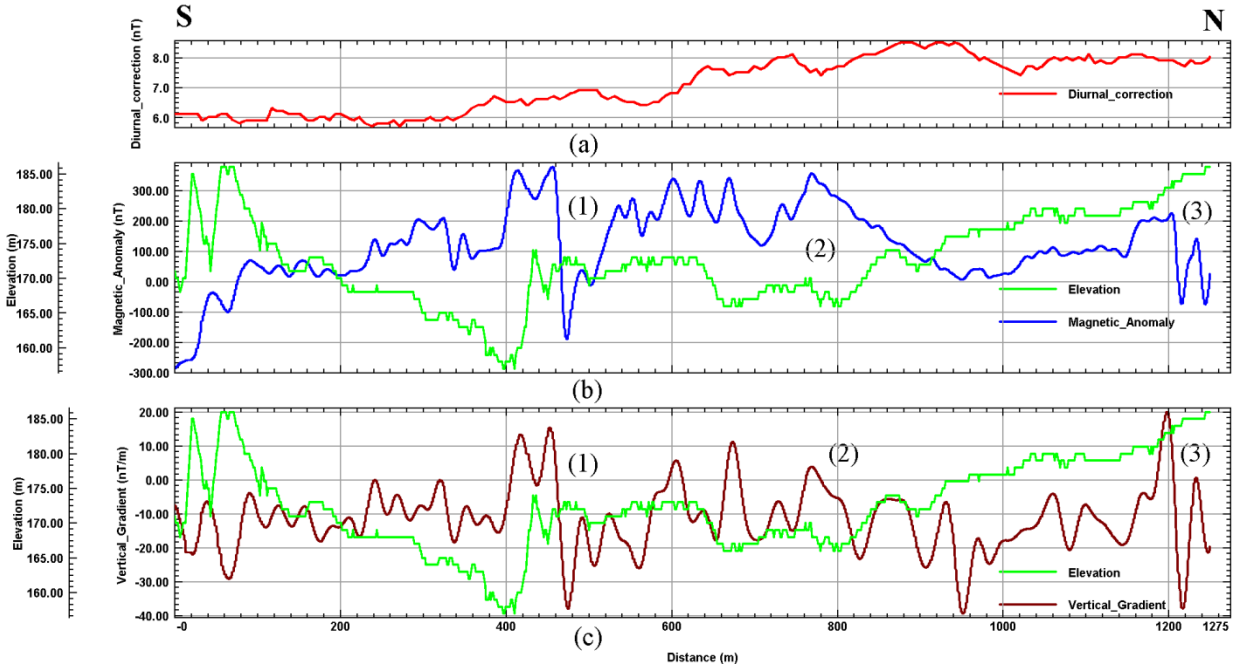

Figure 4.15 *Magnetic Profile 12, (a) Diurnal corrections, (b) magnetic anomaly and (c) vertical gradient of the total magnetic field.*

4.2.13 Profile 13

The profile is almost 1600 meter long and runs parallel to Profile 11 and should cross the Fannefjorden fault. Diurnal variations of the Earth's magnetic field do not exceed 3 nT during the measurements of this profile (Fig. 4.16a). An anomaly with an amplitude of 200 nT is seen ((1) in Fig. 4.16b). Interpretation of the variations in vertical gradient appears to be hampered by a too-high noise level (Fig. 4.16b, c). Nevertheless both magnetic anomaly and vertical gradient show a step in magnitude that can be related to a fault with a significant vertical displacement.

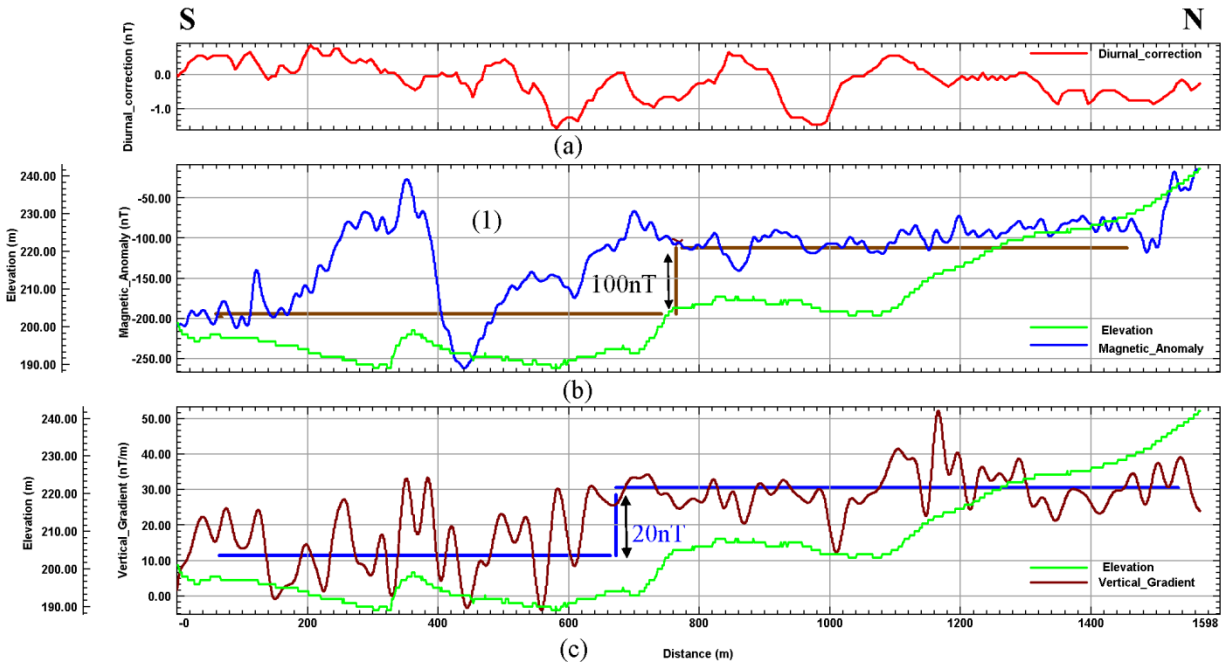

Figure 4.16 *Magnetic Profile 13 (a) Diurnal corrections, (b) magnetic anomaly and (c) vertical gradient of the total magnetic field.*

4.2.14 Profile 14

This profile is the continuation of Profile 13. The modest diurnal variations (i.e. less than 2 nT) are shown in Figure 4.17a. Different magnetic anomalies can be isolated (Fig. 4.17b). The vertical gradient shows two distinct anomalies with higher amplitudes ((2) and (6) in Fig. 4.17c). These two anomalies find their counterparts in the total magnetic field but their amplitude are much more pronounced in the vertical gradient indicating shallow source bodies.

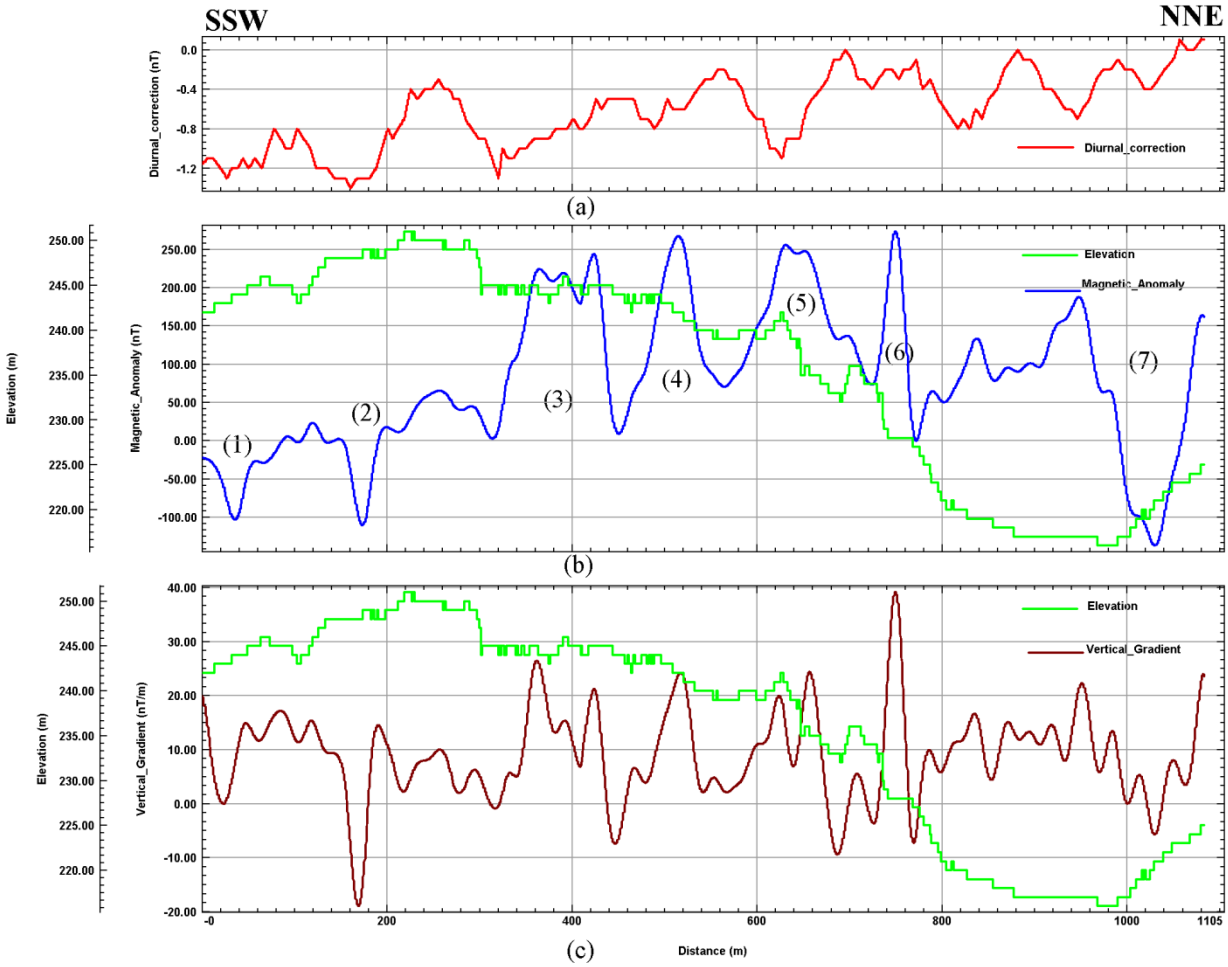

Figure 4.17 *Magnetic Profile 14, (a) Diurnal corrections, (b) magnetic anomaly and (c) vertical gradient of the total magnetic field.*

4.2.15 Profile 15

This profile is located parallel to Profile 13 to verify the anomaly along the latter. Due to a problem with GPS, we were not able to record the profile continously. For diurnal correction data from base magnetometer at Rørvik (RVK) have been used. The station at Rørvik is part of the geomagnetic reference network for Norway (WWW.tgo.uit.no)

Figure 4.18 shows the measurement results. Three anomalies can be detected: (1) is parallel to the anomaly in Profile 13 and its shape and amplitude (200 nT) are similar. (3) depicts an increase in magnetic value which can also be detected in Profile 13. This anomaly with 250 nT amplitude might be related to a fault.

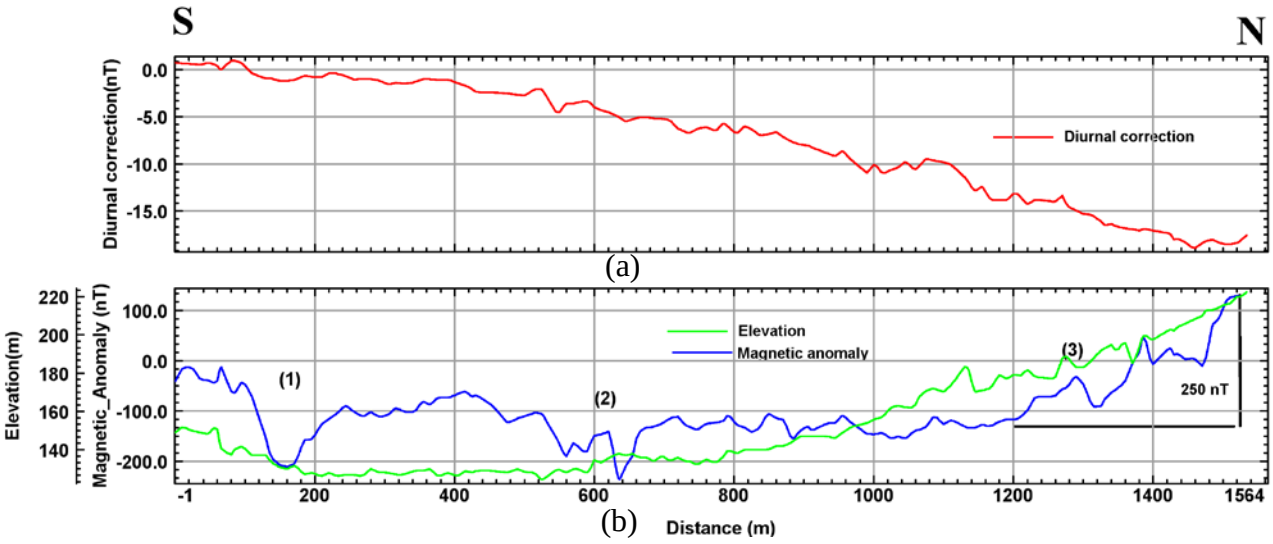

Figure 4.18 *Magnetic Profile 15, (a) Diurnal corrections, (b) magnetic anomaly*

5. DISCUSSION

In the new gravity and magnetic data along Tingvollfjorden anomalies can be observed that possibly relate to segments of the MTFC. We concentrated our measurements in three areas: (1) the Eidsøra region which is located in the middle of a valley and where the Tjellefonna fault zone is the main object, (2) a region close to the Fosterlågen Lake to study the Fannefjorden fault zone and (3) between these two regions for studying possible small faults related to these main segments.

The Bouguer anomaly is calculated by using a density of 2790 kg/m^3. For finding the appropriate density for Bouguer correction, the Nettleton method has been used (Fig. 3.6). The value applied here is conceivably higher than the standard Bouguer density, but in agreement with regional density maps (Olesen et al. 2010). In the valley close to Eidsøra (Fig. 3.5) the gravity data show more negative values, which are interpreted to represent sediments that fill the subsurface down to a few meters. A profile has been extracted from gravity points which shows a step form anomaly (Fig. 3.7).

Magnetic anomalies reflect changes in the Earth's magnetic field and are generally used to infer variations in the magnetization of the bedrock. Various geologic explanations for these anomalies should be considered. In some situations, shallow material underlying the terrain itself may be magnetic and thus produce magnetic anomalies that correlate with topography. The growth of secondary magnetic minerals along concealed fractures or faults could produce linear magnetic anomalies in the study area and probably such processes occurred in our study area. The bedrock map of the study area evidences of such concentrations (Fig 5.1). For example Profiles 5, 6 and 7 are located on top of an amphibolite structure which according to the geological map is an antiform. The magnetic high in Profile 5 (Fig. 4.8) is perpendicular to the axial plane of this body and in the vicinity of this anomaly a fault core outcrop is mapped.

The juxtaposition of lithologies having slightly contrasting magnetic properties may explain the magnetic anomalies (e.g., anomaly numbered (1) in Figures 13 and 15). These contacts may be due to crustal faulting or to depositional processes. Among the conducted profiles, Profile 1, 2, 3 and 8 which have S – N strike show anomalies possibly reflecting fault structures related to

the Tjellefonna fault zone. Profiles 11 and 13 show anomalies which can be related to Fannefjorden fault zone.

These new data will be used for modeling the subsurface geology in the study area and combined with the regional data set of NGU. Developing a 2D and 3D model will be the main aim of the project. For constructing these models the results of other independent methods will be combined. Density and magnetic susceptibility data will be compiled from rock samples gathered from the study area. These data can help determine the sources of gravity and magnetic anomalies and constrain the 2- and 3-D modeling of the potential-field data.

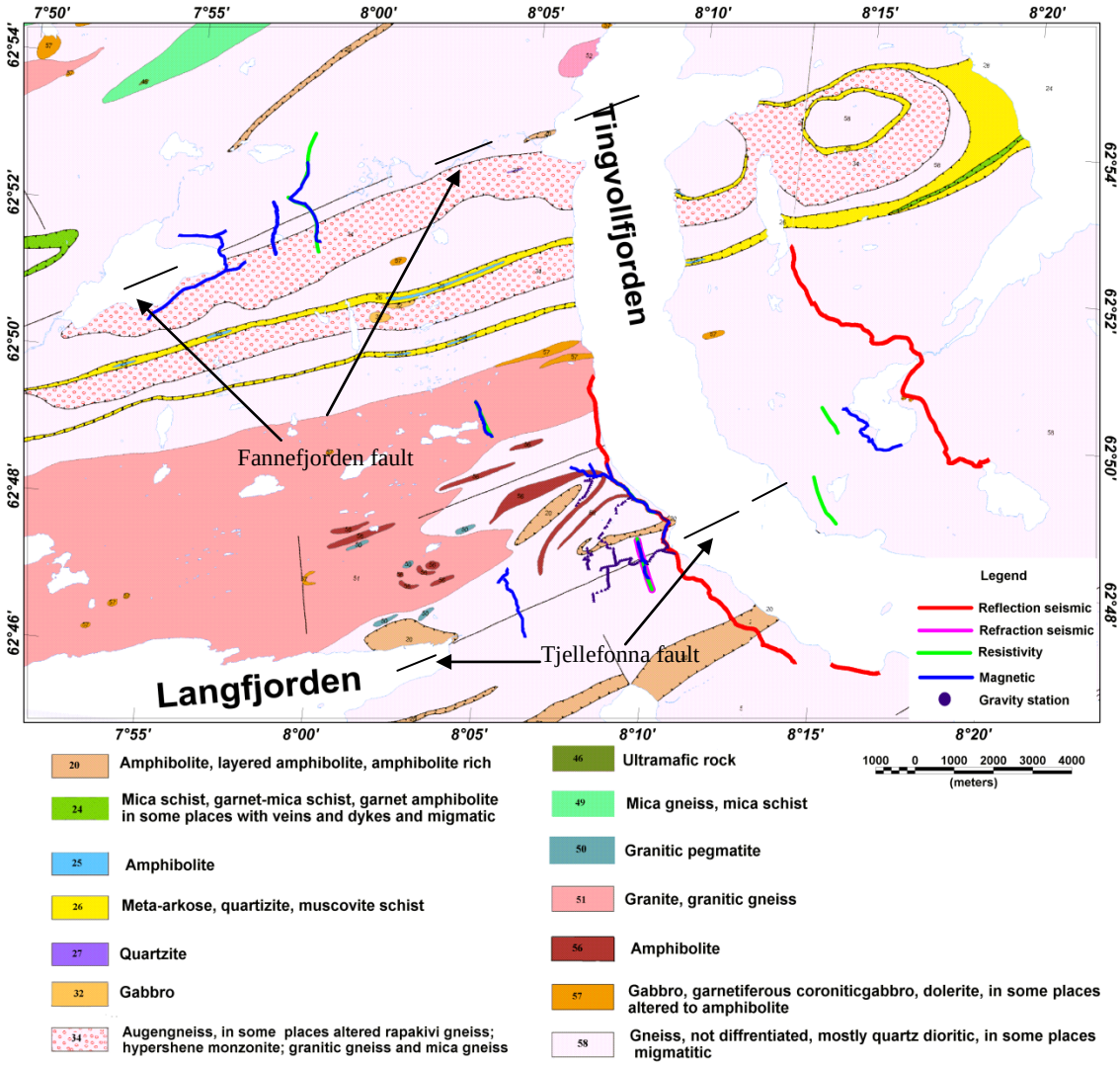

Figure 5.1 *Bedrock map of the study area. Gravity and magnetic surveys depicted as dots and blue lines respectively. The proposed segments of the MTFC, Tjellefonna and Fannefjorden faults, are shown with the dashed, black lines. (Extracted from 1:50 000 bedrock map of Norway (Tvetan et al., 1998).*

6. ACKNOWLEDGMENTS

The presented study is part of the project “The Møre-Trøndelag Fault Complex - an integrated study” funded by the Research Council of Norway and the Geological Survey of Norway and carried out in cooperation between NGU, NTNU and Uppsala University. We would like to thank the Geological Survey of Norway and Uppsala University for providing the field instruments. We are very grateful to all the students who helped us collecting the data, Albert Eyike from University of Douala (Cameroon), Sara Ferrante and Anna Tentor from University of Trieste (Italy), Andrea Biedermann from University of Zurich (ETHZ, Svitzerland), Marit Stokke Bauck, Kurdistan Chawshin, Marianne Aarset and Tore Vattekar from NTNU, Trondheim.

7. REFERENCES

Blakely, R.J. 1995: Potential theory in gravity and magnetic applications: Cambridge University Press, 441.

Gabrielsen, R.H., Odinsen, T., & Grunnaleite, I. 1999: Structuring of the Northern Viking Graben and the Møre Basin; the influence of basement structural grain and the particular role of the Møre Trøndelag Fault Complex. Mar. & Pet. Geol. 16, 443–465.

Grønlie, A., & Roberts, D., 1989: Resurgent strike–slip duple development along the Hitra–Snåsa and Verran faults, Møre–Trøndelag fault zone, central Norway. *J. Struct. Geol.* 11, 295–305.

LaFehr, T.R 1991: An exact solution for the gravity curvature (Bullard B) correction. Geophysics 56, 1179-1184.

Nasuti, A., Chawshin, K., Dalsegg, E., Tønnesen, J.F., Ebbing, J. and Gellein, J., 2009: Electrical resistivity and refraction seismics over a segment of the Møre-Trøndelag Fault Complex. NGU Report 2009.037, 37pp.

Nettleton, L. L. 1939: Determination of density for reduction of gravimeter observations: Geophysics 4, 176–183.

Olesen, O., Brönner, M., Ebbing, J., Gellein, J., Gernigon, L., Koziel, J., Lauritsen, T., Myklebust, R., Sand, M., Solheim, D. and Usov, S. 2010: New aeromagnetic and gravity compilations from Norway and adjacent areas – methods and applications. 7th Petroleum Conference Proceedings, *in press*.

Redfield, T.F., Braathen, A., Gabrielsen, R.H., Osmundsen, P.T., Torsvik, T.H., & Andriessen, P.A.M. 2005: Late Mesozoic to Early Cenozoic components of vertical separation across the Møre–Trøndelag Fault Complex, Norway. Tectonophysics 395, 233– 249.

Redfield, T.F., Osmundsen, P.T. 2009: The Tjellefonna fault system of Western Norway: Linking late-Caledonian extension, post-Caledonian normal faulting, and Tertiary rock column uplift with the landslide-generated tsunami event of 1756, Tectonophysics, 474, 106–123.

Tveten, E., Lutro, O., Thorsnes, T. 1998: Berggrunnskart Ålesund. 1:250000, (Ålesund, western Norway), NGU Trondheim (bedrock map).

Watts, L.M. 2001: The Walls Boundary fault zone and the Møre Trøndelag Fault Complex: a case study of two reactivated fault zones, Department of Geological Sciences, University of Durham Ph.D. Thesis.

APPENDIX – MEASURED GRAVITY POINTS

Station = Station name, Longitude, latitude = geographical coordinates [WGS 84], Elevation = height above mean sea level [m], ABS= Absolute gravity [m/s2], TC= Terrain correction [mGal], FA= Free air anomaly [mGal], BA= Simple Bouguer anomaly [mGal], CBA= Complete Bouguer anomaly [mGal].

Station	Longitude	Latitude	Elevation	ABSG	TC	FA	BA	CBA
A01	8.13401	62.7958	98.42	982072	3.82	-28.64	-40.29	-36.47
A02	8.13387	62.796	99.35	982072	3.85	-28.46	-40.22	-36.37
A03	8.13368	62.7963	101.32	982072	3.88	-28.15	-40.14	-36.27
A04	8.13346	62.7966	104.76	982071	3.88	-27.69	-40.09	-36.21
A05	8.13324	62.7968	109.5	982070	3.87	-27.03	-39.99	-36.11
A06	8.13334	62.7971	113.27	982070	3.91	-26.56	-39.97	-36.05
A07	8.13368	62.7973	117.95	982069	3.89	-26.02	-39.98	-36.08
A08	8.13402	62.7976	123.13	982068	3.97	-25.39	-39.96	-35.99
A09	8.1333	62.7976	127.15	982067	3.94	-24.88	-39.93	-35.99
A10	8.1325	62.7976	132.37	982066	3.82	-24.22	-39.89	-36.07
A11	8.13142	62.7976	138.14	982065	3.73	-23.43	-39.78	-36.06
A12	8.13189	62.7979	143.1	982064	3.66	-22.81	-39.74	-36.08
A13	8.13333	62.7983	152.05	982063	3.77	-21.73	-39.72	-35.96
A14	8.13311	62.7984	154.8	982062	3.71	-21.32	-39.63	-35.92
A15	8.13447	62.7987	166.66	982060	3.64	-20.1	-39.82	-36.19
A16	8.13516	62.7989	173.01	982059	3.63	-19.36	-39.83	-36.2
A17	8.13476	62.7991	175.92	982058	3.5	-18.98	-39.79	-36.29
A18	8.13354	62.7991	180.04	982057	3.48	-18.41	-39.71	-36.23
A19	8.13314	62.7994	186.91	982056	3.39	-17.48	-39.6	-36.21
A20	8.1327	62.7997	194.44	982055	3.35	-16.5	-39.5	-36.15
A21	8.13242	62.8002	204.97	982053	3.35	-15.13	-39.39	-36.04
B01	8.13008	62.8156	121.43	982071	3.2	-23.97	-38.34	-35.14
B02	8.13131	62.8156	124.63	982070	3.33	-23.71	-38.46	-35.13
B03	8.13103	62.8151	124.27	982070	3.3	-23.77	-38.48	-35.18
B04	8.13068	62.8147	124.78	982070	3.27	-23.7	-38.46	-35.19
B05	8.13036	62.8142	125.92	982070	3.27	-23.64	-38.54	-35.27
B06	8.13002	62.8138	126.79	982070	3.26	-23.6	-38.6	-35.34
B07	8.12982	62.8134	125.3	982070	3.31	-23.85	-38.68	-35.37
B08	8.12933	62.8129	123.93	982070	3.29	-24	-38.67	-35.38
B09	8.12898	62.8125	122.62	982070	3.32	-24.25	-38.76	-35.43
B10	8.12858	62.8121	122.97	982070	3.34	-24.26	-38.81	-35.48
B11	8.12824	62.8118	125.03	982070	3.32	-23.94	-38.74	-35.42
B12	8.12741	62.8115	128.24	982069	3.23	-23.44	-38.62	-35.39
B13	8.1262	62.8111	133.61	982068	3.04	-22.63	-38.44	-35.41
B14	8.12562	62.8103	144.97	982066	3.03	-21.22	-38.37	-35.34
B15	8.12475	62.8097	154.55	982064	2.97	-20.05	-38.34	-35.37
C01	8.17069	62.8066	40.11	982082	5.98	-37.54	-42.29	-36.31

C02	8.17049	62.8069	43.18	982081	5.93	-37.07	-42.18	-36.25
C03	8.17051	62.8071	44.6	982081	5.96	-36.94	-42.22	-36.26
C04	8.17075	62.8075	47.68	982081	5.96	-36.55	-42.2	-36.24
C05	8.17124	62.8077	51.31	982080	6.03	-36.33	-42.41	-36.37
C06	8.17166	62.808	55.18	982079	6.25	-36.15	-42.68	-36.43
C07	8.1718	62.8082	56.53	982078	6.4	-36.09	-42.78	-36.38
C08	8.17119	62.8084	57.4	982079	6.32	-35.63	-42.42	-36.1
C09	8.17037	62.8085	59.74	982079	6.26	-35.02	-42.09	-35.83
C10	8.16973	62.8087	58.81	982079	6.24	-35.02	-41.98	-35.75
C11	8.16908	62.8088	59.25	982079	6.24	-34.82	-41.83	-35.59
C12	8.16838	62.809	60.88	982079	6.31	-34.7	-41.9	-35.6
C13	8.16787	62.8093	61.84	982078	6.53	-34.79	-42.11	-35.58
C14	8.16715	62.8097	57.7	982079	6.88	-35.55	-42.38	-35.5
C15	8.16619	62.81	56.25	982079	7.06	-35.93	-42.59	-35.53
C16	8.16535	62.81	60.37	982078	7.13	-35.55	-42.69	-35.57
C17	8.16457	62.8101	62.18	982078	7.18	-35.33	-42.69	-35.51
C18	8.16378	62.8101	65.16	982077	7.19	-34.95	-42.66	-35.46
C19	8.16313	62.8101	69.17	982076	7.13	-34.4	-42.59	-35.45
C20	8.16239	62.8102	70.97	982076	7.03	-34.04	-42.44	-35.41
C21	8.16151	62.8105	71.46	982076	6.85	-33.87	-42.33	-35.48
C22	8.16088	62.8104	72.81	982076	6.76	-33.66	-42.28	-35.52
C23	8.16036	62.8107	72.03	982076	6.73	-33.76	-42.29	-35.56
C24	8.16018	62.8111	69.65	982076	6.88	-34.26	-42.5	-35.62
C25	8.15978	62.8116	69.37	982076	7.31	-34.6	-42.81	-35.5
C26	8.15925	62.8116	67.54	982076	7.14	-34.96	-42.95	-35.81
C27	8.15877	62.8119	64.02	982077	7.39	-35.42	-43	-35.61
C28	8.15797	62.8121	64.64	982077	7.53	-35.36	-43.01	-35.48
C29	8.15716	62.8121	68.59	982076	7.49	-34.91	-43.03	-35.54
C30	8.1564	62.8122	70.3	982076	7.47	-34.58	-42.91	-35.44
C31	8.15557	62.8122	73.12	982075	7.35	-34.2	-42.85	-35.5
C32	8.15486	62.8123	76.27	982075	7.18	-33.75	-42.78	-35.61
C33	8.15403	62.8124	80.16	982074	6.88	-33.05	-42.54	-35.66
C34	8.15346	62.8126	81.67	982074	6.7	-32.63	-42.3	-35.6
C35	8.15283	62.8129	84.72	982074	6.56	-32.21	-42.24	-35.68
C36	8.15248	62.813	86.63	982073	6.52	-32.19	-42.44	-35.92
C37	8.15162	62.8133	90	982073	6.53	-31.74	-42.39	-35.86
C38	8.15096	62.8136	91.2	982073	6.66	-31.66	-42.45	-35.79
C39	8.15031	62.8137	92.13	982072	6.54	-31.47	-42.37	-35.83
C40	8.14985	62.8142	91.66	982072	6.97	-31.84	-42.69	-35.72
C41	8.14954	62.8144	90.14	982072	6.99	-32.22	-42.89	-35.91
C42	8.14859	62.8147	90.95	982072	6.88	-31.9	-42.66	-35.78
C43	8.14786	62.815	91.66	982072	7.15	-32.17	-43.02	-35.86
C44	8.14673	62.8153	90.35	982072	7.17	-32.22	-42.91	-35.74
C45	8.14568	62.8154	91.31	982072	6.92	-31.81	-42.61	-35.7
C46	8.14457	62.8156	90.55	982073	6.41	-31.35	-42.07	-35.66

C47	8.14354	62.8159	90.17	982073	6.21	-31.27	-41.94	-35.73
C48	8.14257	62.8162	90.49	982074	6.01	-30.94	-41.65	-35.64
C49	8.14141	62.8164	89.57	982074	5.67	-30.7	-41.3	-35.63
C50	8.14	62.8167	98.04	982073	5.36	-29.03	-40.63	-35.27
C51	8.13861	62.8171	106.01	982072	5.2	-27.81	-40.35	-35.15
C52	8.13705	62.8174	114.96	982071	4.93	-26.49	-40.09	-35.16
C53	8.13593	62.8174	122.99	982070	4.58	-25.08	-39.63	-35.05
C54	8.13479	62.8168	127.82	982069	4.07	-24.03	-39.16	-35.09
C55	8.13322	62.8165	127.24	982070	3.71	-23.71	-38.77	-35.06
C56	8.13169	62.8163	122.58	982071	3.41	-24	-38.51	-35.09
C57	8.1301	62.816	119.29	982072	3.22	-24.18	-38.3	-35.08
C58	8.12888	62.8155	118.79	982072	3.1	-24.14	-38.2	-35.09
C59	8.12782	62.8155	117.03	982072	3.05	-24.2	-38.05	-35.01
D01	8.14585	62.7999	124.9	982067	3.97	-25.35	-40.13	-36.16
D02	8.14572	62.8002	132.54	982066	3.94	-24.4	-40.08	-36.14
D03	8.14561	62.8007	144.71	982064	3.87	-22.83	-39.96	-36.09
D04	8.14402	62.8008	156.69	982062	3.67	-21.25	-39.79	-36.12
D05	8.14298	62.8008	164.14	982060	3.54	-20.31	-39.74	-36.2
D06	8.14226	62.801	173.61	982059	3.38	-19.11	-39.65	-36.27
D07	8.14222	62.8015	181.4	982057	3.34	-18.11	-39.57	-36.23
D08	8.14124	62.802	189.94	982056	3.24	-16.85	-39.33	-36.08
D09	8.13965	62.8021	205.86	982053	3.26	-15	-39.36	-36.1
D10	8.13923	62.8022	210.36	982052	3.27	-14.31	-39.2	-35.93
D11	8.13803	62.8027	222.91	982050	3.29	-12.75	-39.13	-35.84
D12	8.13773	62.8029	223.54	982050	3.22	-12.69	-39.14	-35.92
D13	8.1383	62.8034	223.57	982050	3.2	-12.84	-39.29	-36.09
D14	8.13888	62.8038	223.53	982050	3.2	-12.92	-39.37	-36.17
D15	8.13928	62.804	220.41	982050	3.16	-13.2	-39.28	-36.12
D16	8.1402	62.8052	209.37	982053	3.06	-14.28	-39.06	-36
D17	8.14108	62.8057	214.23	982052	3.16	-13.98	-39.33	-36.17
D18	8.14165	62.8065	210.31	982053	3.21	-14.19	-39.08	-35.87
D19	8.14213	62.807	210.36	982053	3.29	-14.11	-39	-35.7
D20	8.14247	62.8073	210.92	982053	3.35	-14	-38.95	-35.61
D29	8.14509	62.8089	204.75	982053	3.82	-15.74	-39.97	-36.15
D30	8.14482	62.8095	202.64	982054	3.98	-15.98	-39.95	-35.97
D31	8.14458	62.81	200.42	982054	4.05	-16.63	-40.35	-36.3
D32	8.14558	62.8107	188.16	982056	4.37	-18.05	-40.31	-35.94
D33	8.1473	62.811	174.89	982058	4.75	-19.8	-40.5	-35.75
D34	8.14787	62.8114	167.26	982060	4.94	-21.06	-40.85	-35.91
D35	8.14888	62.8118	151.95	982062	5.23	-23.16	-41.14	-35.91
D40	8.15022	62.8125	124.6	982067	5.66	-26.92	-41.67	-36.01
D41	8.15106	62.8127	114.26	982069	6.01	-28.44	-41.96	-35.95
D42	8.15239	62.8124	102.56	982070	6.28	-30.11	-42.25	-35.96
E01	8.17237	62.8023	2.27	982089	5.88	-42.16	-42.43	-36.55
E010	8.16993	62.8036	10.1	982088	5.61	-40.84	-42.03	-36.42

E011	8.16996	62.804	12.7	982087	5.59	-40.52	-42.02	-36.43
E012	8.16971	62.8042	14.63	982087	5.61	-40.2	-41.93	-36.32
E013	8.16956	62.8044	16.9	982087	5.63	-39.84	-41.85	-36.22
E014A	8.16976	62.8047	17.64	982087	5.69	-39.73	-41.81	-36.13
E015	8.16975	62.8049	19.57	982086	5.71	-39.55	-41.87	-36.16
E015A	8.16981	62.8052	21.96	982086	5.73	-39.27	-41.87	-36.14
E015B	8.16979	62.8051	20.79	982086	5.72	-39.43	-41.89	-36.17
E015C	8.16976	62.8054	22.88	982085	5.76	-39.21	-41.92	-36.16
E016	8.1699	62.8055	23.91	982085	5.78	-39.17	-42	-36.22
E016A	8.16996	62.8055	26.33	982085	5.78	-38.91	-42.02	-36.25
E016B	8.16957	62.8057	27.22	982084	5.82	-38.86	-42.08	-36.26
E016C	8.1698	62.8055	25.18	982085	5.8	-39.01	-41.99	-36.19
E017	8.17	62.8059	28.67	982084	5.84	-38.72	-42.11	-36.28
E017A	8.16999	62.806	31.94	982084	5.84	-38.35	-42.13	-36.3
E018	8.17025	62.8063	33.87	982083	5.86	-38.2	-42.21	-36.34
E019	8.17062	62.8064	38.43	982082	5.96	-37.77	-42.31	-36.36
E03	8.17198	62.8025	2.02	982089	5.81	-42.15	-42.38	-36.57
E04	8.1722	62.8027	2.24	982089	5.79	-42.17	-42.44	-36.65
E05	8.17218	62.8029	2.37	982089	5.75	-42.17	-42.45	-36.7
E06	8.17167	62.8031	3.32	982089	5.71	-41.99	-42.38	-36.68
E07	8.17121	62.8033	5.58	982088	5.68	-41.65	-42.31	-36.64
E08	8.17072	62.8034	7.32	982088	5.65	-41.29	-42.15	-36.51
E09	8.17009	62.8035	8.28	982088	5.64	-41.06	-42.04	-36.4
E20	8.17143	62.8023	3.19	982089	5.84	-41.91	-42.29	-36.45
E21	8.17101	62.8019	7.13	982088	5.84	-41.37	-42.21	-36.38
E22	8.17073	62.8016	11.74	982087	5.8	-40.77	-42.16	-36.36
E23	8.17018	62.8015	14.17	982087	5.74	-40.44	-42.12	-36.37
E24	8.16941	62.8016	16.05	982086	5.66	-40.13	-42.03	-36.37
E25	8.16867	62.8015	17.4	982086	5.64	-39.95	-42.01	-36.38
E26	8.16794	62.8014	19.5	982086	5.62	-39.69	-42	-36.38
E27	8.17053	62.8014	13.44	982087	5.79	-40.59	-42.18	-36.39
E28	8.1715	62.8013	11.05	982087	5.94	-40.99	-42.3	-36.37
E29	8.17248	62.8013	9.04	982087	6.05	-41.37	-42.44	-36.39
E30	8.17348	62.8012	8.16	982087	6.16	-41.66	-42.62	-36.46
E31	8.17448	62.8012	8.07	982087	6.23	-41.8	-42.76	-36.53
E32	8.17542	62.8012	8.87	982087	6.3	-41.89	-42.94	-36.65
E33	8.17618	62.8011	10.67	982086	6.37	-41.84	-43.1	-36.73
E34	8.16708	62.8011	22.08	982085	5.69	-39.42	-42.04	-36.35
E35	8.16642	62.8008	25.28	982085	5.59	-38.97	-41.96	-36.38
E36	8.16585	62.8004	27.63	982084	5.58	-38.8	-42.07	-36.5
E37	8.16549	62.8	31.26	982083	5.6	-38.47	-42.17	-36.58
E38	8.16479	62.7997	33.28	982083	5.58	-38.35	-42.29	-36.72
E39	8.16432	62.7993	35.43	982082	5.64	-38.23	-42.42	-36.77
E40	8.16404	62.7988	37.65	982082	5.78	-37.95	-42.41	-36.63
E41	8.16283	62.7986	41.14	982081	5.61	-37.37	-42.23	-36.62

E42	8.16201	62.7986	43.34	982081	5.54	-37.01	-42.14	-36.6
E43	8.16137	62.7988	45.62	982080	5.38	-36.73	-42.13	-36.75
E44	8.16046	62.7987	48	982080	5.32	-36.38	-42.06	-36.74
E45	8.15968	62.7986	50.35	982080	5.26	-35.93	-41.89	-36.64
E46	8.15903	62.7985	52.72	982079	5.18	-35.53	-41.77	-36.59
E47	8.15827	62.7981	55.41	982079	5.17	-35.26	-41.82	-36.65
E48	8.15765	62.798	57.98	982078	5.12	-34.89	-41.75	-36.63
E49	8.15696	62.7977	60.21	982078	5.09	-34.61	-41.73	-36.64
E50	8.15619	62.7976	62.04	982078	5.06	-34.31	-41.65	-36.59
E51	8.15556	62.7975	64.29	982077	5.01	-33.91	-41.52	-36.51
E52	8.15458	62.7976	66.8	982077	4.9	-33.25	-41.16	-36.26
E53	8.15423	62.7979	68.01	982077	4.86	-33.01	-41.06	-36.2
E54	8.15425	62.7982	69.93	982077	4.79	-32.63	-40.9	-36.12
E55	8.15468	62.7986	72	982077	4.71	-32.32	-40.84	-36.13
E56A	8.15507	62.799	74.55	982076	4.64	-32.02	-40.85	-36.21
E57	8.15456	62.7989	76.02	982076	4.61	-31.73	-40.72	-36.12
E58	8.15395	62.7989	77.6	982076	4.59	-31.5	-40.69	-36.1
E59	8.15297	62.7987	80.51	982075	4.54	-31.07	-40.6	-36.05
E60	8.15206	62.7985	83.22	982075	4.48	-30.74	-40.59	-36.11
E61	8.15116	62.7984	85.94	982074	4.39	-30.43	-40.6	-36.21
E62	8.15026	62.7983	88.09	982074	4.33	-30.09	-40.52	-36.19
E63	8.14936	62.7981	90.87	982073	4.24	-29.72	-40.48	-36.24
E64	8.1489	62.7977	93.73	982073	4.18	-29.4	-40.49	-36.32
E65	8.14853	62.7974	95.42	982072	4.15	-29.25	-40.54	-36.39
E66	8.14784	62.7971	97.74	982072	4.09	-28.99	-40.56	-36.46
E67	8.14768	62.7973	97.11	982072	4.07	-28.95	-40.44	-36.37
E68	8.14754	62.7975	97.78	982072	4.04	-28.8	-40.37	-36.33
E69	8.14738	62.7978	98.61	982072	4.03	-28.6	-40.27	-36.23
E70	8.14728	62.798	99.72	982072	4.03	-28.39	-40.2	-36.17
E71	8.14716	62.7982	101.29	982072	4.02	-28.16	-40.15	-36.13
E72	8.147	62.7984	102.97	982072	4.01	-27.92	-40.11	-36.1
E73	8.14683	62.7986	104.58	982071	4.01	-27.71	-40.09	-36.08
E74	8.14667	62.7988	106.99	982071	4	-27.43	-40.09	-36.09
E75	8.14666	62.7991	110.31	982070	3.99	-27.07	-40.13	-36.14
E76	8.14652	62.7993	113.59	982070	3.98	-26.61	-40.06	-36.08
E77	8.14627	62.7995	117.84	982069	3.98	-26.05	-40	-36.02
E78	8.14601	62.7997	122.16	982068	3.98	-25.53	-39.99	-36
F01	8.14723	62.797	98.5	982072	4.06	-28.88	-40.54	-36.48
F02	8.14627	62.7969	98.89	982072	4.03	-28.84	-40.55	-36.52
F03	8.14529	62.7967	99.59	982072	4	-28.7	-40.49	-36.49
F04	8.14432	62.7966	100.08	982072	3.98	-28.61	-40.45	-36.47
F05	8.14339	62.7965	100.96	982072	3.96	-28.42	-40.36	-36.4
F06	8.14244	62.7964	101.47	982071	3.94	-28.28	-40.29	-36.35
F07	8.1415	62.7962	101.04	982071	3.93	-28.41	-40.37	-36.44
F08	8.14062	62.796	100.76	982072	3.92	-28.42	-40.34	-36.42

F09	8.14038	62.7955	101.17	982071	3.95	-28.35	-40.33	-36.38
F10	8.14378	62.7962	101.74	982071	3.96	-28.38	-40.42	-36.46
F11	8.14381	62.796	103.02	982071	3.96	-28.26	-40.45	-36.49
F12	8.14393	62.7958	102.89	982071	4	-28.33	-40.5	-36.51
F13	8.14395	62.7955	102.14	982071	4.03	-28.42	-40.51	-36.48
F130	8.14471	62.7916	121.46	982067	4.85	-26.39	-40.76	-35.91
F131	8.14364	62.7912	123.16	982067	4.91	-26.17	-40.75	-35.84
F132	8.14186	62.7908	127.11	982066	4.8	-25.65	-40.69	-35.89
F133	8.13973	62.7903	130.67	982065	4.68	-25.05	-40.51	-35.84
F14	8.14402	62.7953	100.54	982071	4.09	-28.75	-40.65	-36.56
F15	8.14407	62.7951	101.63	982071	4.11	-28.43	-40.46	-36.35
F16	8.14412	62.7949	102.34	982071	4.13	-28.41	-40.52	-36.39
F17	8.14419	62.7946	102.63	982071	4.16	-28.39	-40.53	-36.37
F18	8.14425	62.7944	102.88	982071	4.21	-28.39	-40.57	-36.36
F19	8.14434	62.7942	103.58	982071	4.24	-28.32	-40.58	-36.33
F20	8.14429	62.794	104.55	982070	4.27	-28.19	-40.56	-36.29
F21	8.14437	62.7938	105.93	982070	4.31	-28.07	-40.61	-36.3
F22	8.14442	62.7936	107.52	982070	4.36	-27.81	-40.53	-36.18
F23	8.14445	62.7934	108.99	982070	4.39	-27.61	-40.51	-36.12
F24	8.14468	62.7932	109.77	982069	4.46	-27.54	-40.53	-36.07
F25	8.14484	62.7929	110.87	982069	4.53	-27.4	-40.52	-35.99
F26	8.14499	62.7927	112	982069	4.6	-27.33	-40.58	-35.98
F27	8.14514	62.7925	113.18	982069	4.68	-27.23	-40.62	-35.94
F28	8.14525	62.7922	114.92	982068	4.75	-27.07	-40.67	-35.91
F29	8.14527	62.792	117.33	982068	4.81	-26.83	-40.72	-35.91
F35	8.16331	62.7981	48.82	982080	5.68	-36.31	-42.09	-36.41
H01	8.13776	62.79	132.77	982065	4.6	-24.75	-40.46	-35.87
H02	8.13808	62.7896	136.56	982064	4.7	-24.37	-40.53	-35.83
H03	8.13822	62.7892	140.17	982063	4.81	-24.03	-40.62	-35.81
H04	8.13843	62.7888	145.51	982062	4.94	-23.57	-40.78	-35.85
H05	8.13865	62.7883	151.46	982061	5.08	-23.06	-40.98	-35.9
J01	8.13446	62.7956	98.55	982072	3.8	-28.75	-40.41	-36.61
J02	8.13422	62.7955	98.36	982072	3.8	-28.77	-40.41	-36.62
L01	8.12772	62.8154	122	982072	3.03	-22.82	-37.26	-34.22
L02	8.12254	62.8201	120	982073	3.12	-22.92	-37.12	-34
L03	8.12006	62.8255	134	982070	3.5	-21.57	-37.42	-33.92
L04	8.12013	62.8289	112	982074	3.93	-24.85	-38.1	-34.17
L05	8.12672	62.8116	138	982069	3.01	-20.17	-36.5	-33.49
L06	8.12084	62.8076	156	982067	2.71	-16.94	-35.4	-32.69
L07	8.1192	62.8026	143	982067	2.59	-20.04	-36.96	-34.37
L08	8.12037	62.7964	107	982073	3.28	-25.47	-38.14	-34.86
L09	8.12406	62.793	95	982074	3.72	-27.48	-38.72	-35
L10	8.15694	62.7961	67.52	982077	5.45	-33.63	-41.63	-36.17
L11	8.17304	62.8006	22	982085	6.11	-39.82	-42.42	-36.31
L12	8.18526	62.7999	17	982085	7.27	-41.17	-43.18	-35.91

L13	8.20174	62.7981	11	982084	6.88	-43.82	-45.12	-38.24